ELSEVIER

Chemical Geology 211 (2004) 185–215

CHEMICAL GEOLOGY
INCLUDING
ISOTOPE GEOSCIENCE

www.elsevier.com/locate/chemgeo

Trace element variations in clinopyroxene and amphibole from alkaline to peralkaline syenites and granites: implications for mineral–melt trace-element partitioning☆

Michael Marks, Ralf Halama, Thomas Wenzel, Gregor Markl*

Institut für Geowissenschaften, AB Mineralogie und Geodynamik, Eberhard-Karls-Universität Tübingen, Wilhelmstraße 56, Tübingen D-72074, Germany

Received 26 November 2003; accepted 6 June 2004

Abstract

Trace element compositions of clinopyroxene and amphibole from three rift-related alkaline to peralkaline igneous complexes (syenites and granites) in South Greenland reflect evolving magma composition as well as crystal-chemical control on partitioning. Clinopyroxenes and amphiboles evolve from Ca–Mg-dominated members via intermediate to Na–Fe^{3+}-dominated members. Most trace elements are highly enriched compared to primitive mantle values, consistent with the highly fractionated character of the host rocks. High field strength element (HFSE; Ti, Zr, Hf, Sn, Nb, Ta) abundances appear to be mainly controlled by the major element composition of the host crystal, which in turn determines the crystal site parameters. A crystal-chemical control is also indicated for the REE, since clinopyroxenes and amphiboles show continuous change from LREE-enriched patterns in the calcic minerals via wave-shaped pattern in the Ca–Na minerals towards a more pronounced HREE enrichment in the most Na-rich minerals. The low absolute abundances of large ion lithophile elements (Ba, Sr, Pb, Eu^{2+}) are interpreted to reflect both a crystal-chemical aversion to incorporate these elements and the effects of prolonged feldspar fractionation on the melt composition. Eu and Pb abundances are also affected by oxygen fugacity and crustal assimilation, respectively.

The partitioning of most trace elements between clinopyroxene and co-genetic amphibole is independent of melt composition or major element composition of the crystals. Most incompatible trace elements (particularly Nb, Ta, U, Th, Rb, Ba and Li) show a slight preference for amphibole. Exceptions to this general trend occur in rocks affected by late-stage fluid circulation resulting in the redistribution of some mobile elements.

Calculation of trace-element compositions of coexisting melts using published partition coefficients for alkaline systems shows that melt compositions similar to whole-rock compositions are obtained for clinopyroxenes with broadly augitic to diopsidic compositions. There is a considerable mismatch between calculated melt and whole-rock data for various elements, i.e., Zr, Hf and the HREE, when melt compositions are calculated from $NaFe^{3+}$-rich aegirine–augites and aegirines. Melt

☆ This is contribution to the mineralogy of Ilímaussaq No. 122.

* Corresponding author. Tel.: +49 7071/29 72 930; fax: +49 7071/29 30 60.
E-mail address: markl@uni-tuebingen.de (G. Markl).

doi:10.1016/j.chemgeo.2004.06.032

compositions from amphiboles also show only limited overlap with whole-rock data. The reasons for these differences may include the following: (1) The crystallization history of the rocks is very complex so that trace element partitioning cannot be expressed with a single partition coefficient. (2) Published mineral–melt partition coefficients cannot generally be applied due to compositional differences between the alkaline to peralkaline systems of this study and the previous studies. (3) Whole-rocks do not reflect melt compositions.

Using a theoretical model of clinopyroxene–melt trace element partitioning based on the crystal chemistry alone, we show that absolute values of D_{REE} decrease but the relative preference for HREE increases as the crystal becomes more aegirine-rich, which is in qualitative accordance with the observed REE patterns. Melts calculated from the theoretically determined partition coefficients show a good overlap with whole-rock data for relatively Fe^{3+}-poor clinopyroxene compositions. Melts calculated from aegirines do not agree with whole-rock compositions, suggesting that the theoretical model needs refinements for the previously not considered incorporation of the $NaFe^{3+}Si_2O_6$ component.

Keywords: Trace element variation; Clinopyroxene; Amphibole; Mineral–melt trace element partitioning

1. Introduction

Trace element data can be used to model and interpret magmatic processes (e.g., Schiano et al., 1993; Walter et al., 1995; Costa et al., 2003). In situ determination of trace elements in minerals has become increasingly popular and many studies have been published on basaltic systems (e.g., Jeffries et al., 1995; Benoit et al., 1996; Coogan et al., 2000; Thompson and Malpas, 2000; Tiepolo et al., 2002), on ultramafic mantle rocks and on phases relevant to mantle melting (e.g., Nimis and Vannucci, 1995; Blundy and Dalton, 2000, Grègoire et al., 2000; Tiepolo et al., 2000a). Studies of trace element partitioning and trace element contents in more evolved silicic systems are less frequent (Lemarchand et al., 1987; Wood and Trigila, 2001), and especially the trace element concentrations of mineral phases in alkaline silicate plutonic rocks have only been studied in a few cases (Larsen, 1979; Wörner et al., 1983; Shearer and Larsen, 1994). Unfortunately, experimental trace element partitioning studies between mafic minerals and alkaline silicate melts are rare. Recent studies based on theoretical models have shown that the crystal chemistry exerts a major control on trace element partitioning (Blundy and Wood, 1991, 1994, 2003; Wood and Blundy, 1997, 2001). However, a number of studies also indicate that melt composition influences trace element partitioning (e.g., Adam and Green, 2003; Bennett et al., 2003).

In this study, we compare the trace element contents of mafic minerals from three related, but petrologically different alkaline to peralkaline igneous complexes in order to investigate the partitioning behavior of trace elements in natural alkaline silicate melts. Our study is focused on clinopyroxene and amphibole because these two minerals can incorporate large amounts of geochemically relevant trace elements (Wood and Blundy, 1997; Bottazzi et al., 1999). The three complexes studied show an almost continuous spectrum in mafic mineral compositions from Ca–Mg-rich and Na-poor to Ca-poor and Na–Fe^{3+}-rich. This enables us to relate relative trace element abundances in the minerals to their crystal chemistry. Furthermore, we determine distribution coefficients between clinopyroxene and amphibole for a wide range of elements in alkaline igneous rocks and compare them with literature data for other rock types. Finally, we use a range of partition coefficients from the literature determined for natural alkaline rocks (Larsen, 1979; Wörner et al., 1983; Lemarchand et al., 1987) to evaluate if they are applicable for the rocks studied here.

2. Regional geology

The Gardar Igneous Province (Fig. 1) in South Greenland represents a failed rift structure of Mid-Proterozoic (1.35–1.14 Ga) age (Upton and Emeleus, 1987; Upton et al., 2003). It comprises a sequence of interlayered basalts and sandstones, a large number of dike rocks of variable chemical composition and 12 major alkaline to peralkaline igneous complexes. The

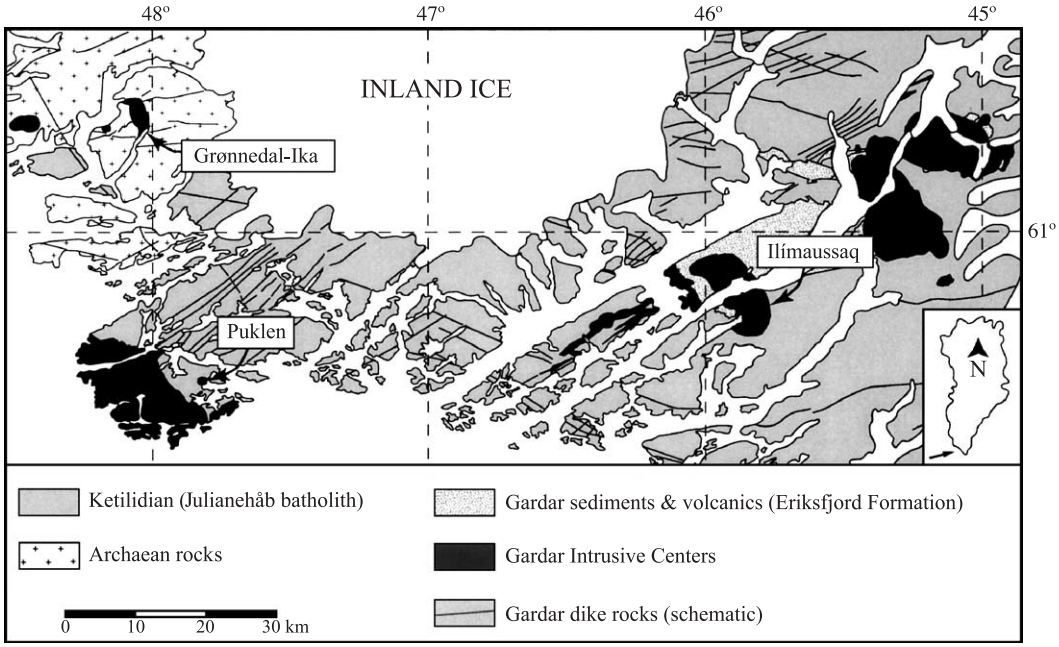

Fig. 1. Sketch map of the alkaline igneous Gardar Province, South Greenland, with the three igneous complexes Puklen, Ilímaussaq and Grønnedal-Ika (modified after Escher and Watt, 1976).

basement rocks mainly consist of I-type calc-alkaline plutonic rocks (Julianehåb batholith) (Van Breemen et al., 1974; Allaart, 1976; Kalsbeek and Taylor, 1985) of Ketilidian (1.85–1.80 Ga) age (Garde et al., 2002). Archaean country rocks occur in the northwestern part of the province. The igneous complexes are mostly composite and show a range from relatively primitive gabbroic to highly evolved syenitic rocks. Fluid inclusion data (Konnerup-Madsen and Rose-Hansen, 1984) and the preserved contacts between supracrustal rocks and the Ilímaussaq intrusion (Poulsen, 1964) show that the magmas intruded into shallow crustal levels (<5 km).

For this study, we selected three igneous complexes: (1) The Puklen complex evolved from silica-saturated syenites to peralkaline granites and represents a silica-oversaturated fractionation trend (Pulvertaft, 1961; Parsons, 1972; Marks et al., 2003). (2) The Ilímaussaq complex, evolving from alkaline, SiO_2-saturated syenites towards agpaitic nepheline syenites, represents the silica-undersaturated trend (Larsen and Sørensen, 1987; Markl et al., 2001b). (3) The Grønnedal-Ika complex represents an association of SiO_2-undersaturated syenite with carbonatite (Emeleus, 1964; Pearce et al., 1997a,b; Halama et al., in press). In the following, we briefly review the petrogenesis of these three complexes.

2.1. The Puklen complex

The field geology of the Puklen complex (Fig. 1) was described in detail by Pulvertaft (1961) and Parsons (1972), and the petrology and geochemistry were investigated by Marks et al. (2003). The first magma pulse formed a suite of silica-saturated to oversaturated syenites, which are cut by a fine-grained and leucocratic granophyre. A second pulse of magma produced a peralkaline granite, which grades into, or may be locally intruded by, fine-grained and leucocratic microgranite. The primary mafic silicates in syenites are augite, olivine and calcic to sodic–calcic amphibole I. Secondary calcic amphibole II formed by late-stage autometasomatic reactions. In the granites, the primary mafic silicate is sodic amphibole, which is overgrown by late-stage aegirine. Detailed isotopic work (Marks et al., 2003) showed that the Puklen melts were primarily derived from a mantle source with variable amounts of crustal contamination.

2.2. The Ilímaussaq complex

The formation of the Ilímaussaq complex (Fig. 1) involved three magma batches (Larsen and Sørensen, 1987; Konnerup-Madsen and Rose-Hansen, 1984). The earliest is represented by augite syenite, which was later intruded by peralkaline granite. The third intrusive phase comprises the major part of the complex and consists of different varieties of partly layered agpaitic nepheline syenites (Ferguson, 1964). The major mafic silicates in the augite syenite are augite, olivine and calcic amphibole (Larsen, 1976, 1977, 1981; Markl et al., 2001a,b; Marks and Markl, 2001). In the alkali granite and in the agpaites, sodic amphibole and aegirine occur in addition to high amounts of eudialyte (REE-rich Zr-silicate). Homogeneous oxygen and neodymium isotope compositions of mineral separates indicate a closed system evolution of the complex and support a mantle derivation of the magma (Marks et al., 2004). The only exception is the peralkaline granite, which is explained by higher amounts of crustal contamination compared to the other rock types (Marks et al., 2004).

2.3. The Grønnedal-Ika complex

The Grønnedal-Ika complex consists of partly layered silica-undersaturated nepheline syenites, which were intruded by a central plug of calciocarbonatite (Emeleus, 1964; Bedford, 1989; Pearce et al., 1997a,b). The major mafic silicate in the nepheline syenites is clinopyroxene, whereas amphibole is very scarce (Bedford, 1989). The nepheline syenitic magmas of the Grønnedal-Ika intrusion are thought to be produced by fractional crystallization of mafic magmas. Sr and Nd isotopic data indicate a fairly homogeneous mantle source for the syenitic and carbonatitic magmas with no significant crustal contamination (Pearce et al., 1997a; Halama et al., in press).

3. Sample material and analytical methods

Several representative samples from each rock type of each of the three intrusions were investigated for this study. Most of these samples have been part of previous petrological and geochemical studies (Markl et al., 2001b; Marks and Markl, 2001; Markl and Baumgartner, 2002; Marks et al., 2003, 2004; Halama et al., in press). Selected samples and minerals analyzed are summarized in Table 1.

Table 1
Summary of samples and minerals analyzed

Rock type	Sample	Analyzed mafic minerals
Ilímaussaq		
Augite syenite	GM1331	augite, calcic amphibole
Augite syenite	GM1333	augite, calcic amphibole
Alkali granite	GM1303	aegirine, sodic amphibole
Agpaite	GM1294	aegirine
Agpaite	GM1305	aegirine
Agpaite	GM1334	aegirine, sodic amphibole
Agpaite	GM1336	aegirine
Agpaite	GM1337	aegirine, sodic amphibole
Agpaite	GM1344	aegirine
Agpaite	GM1347	aegirine, sodic amphibole
Agpaite	GM1370	aegirine, sodic amphibole
Agpaite	GM1371	aegirine
Agpaite	GM1396	sodic amphibole
Late-stage vein	GM1401	sodic amphibole
Pegmatite	GM1657	sodic amphibole
Puklen		
Syenite	GM1586	augite, calcic amphibole I
Syenite	GM1589	calcic amphibole I, calcic amphibole II
Syenite	GM1590	augite, calcic amphibole I
Syenite	GM1600	augite, calcic amphibole I, calcic amphibole II
Syenite	GM1603	augite, calcic amphibole I, calcic amphibole II
Syenite	GM1615	augite, sodic–calcic amphibole
Syenite	GM1616	augite, sodic–calcic amphibole
Syenite	GM1635	augite
Granophyre	GM1593	calcic amphibole I, calcic amphibole II
Alkali granite	GM1587	aegirine, sodic amphibole
Alkali granite	GM1605	aegirine, sodic amphibole
Alkali granite	GM1608	aegirine
Microgranite	GM1620	aegirine, sodic amphibole
Microgranite	GM1627	aegirine, sodic amphibole
Grønnedal-Ika		
Nepheline syenite	GR01	aegirine–augite
Nepheline syenite	GR13	aegirine–augite
Nepheline syenite	GR15	aegirine–augite
Nepheline syenite	GR44	aegirine–augite
Nepheline syenite	GR63	aegirine–augite
Nepheline syenite	GM1496	aegirine–augite
Nepheline syenite	GM1526	aegirine–augite, sodic–calcic amphibole
Nepheline syenite	GM1531	sodic–calcic amphibole

In situ laser ablation inductively coupled plasma-mass spectrometer (LA-ICP-MS) analyses of REE and other trace elements were performed at the EU Large-Scale Geochemical Facility (University of Bristol) using a VG Elemental PlasmaQuad 3+S-Option ICP-MS equipped with a 266-nm Nd-YAG laser (VG MicroProbe II). The laser beam diameter at the sample surface was approximately 20 μm. All measurements were made using Thermo Elemental PlasmaLab "time-resolved analysis" (TRA) data acquisition software with a total acquisition time of 100 s per analysis, allowing about 40 s for background followed by 50 s for laser ablation. NIST 610 (Pearce et al., 1997b) glass was used for instrument calibration, and NIST 612 was used as a secondary standard. Accepted trace element concentrations for both standards and measured concentrations for NIST 612 during the course of this study are given in Table 2. Si was used as an internal standard to correct the ablation yield differences between and during individual analyses on both standards and samples. To avoid analytical uncertainties due to variations in the concentrations of the internal standard, Si concentrations were quantitatively measured within 20 μm of the laser ablation pits using a JEOL 8900 electron microprobe (EMP) at the Universität Tübingen (see below). The precision of trace element concentrations, based on

Table 2
Accepted trace element concentrations (in ppm) for NIST 610 and NIST 612 (Pearce et al., 1997b) and measured concentrations for NIST 612 during the course of this study

Trace element	NIST 610	NIST 612	Measured October 2000	Measured October 2000	Measured October 2001	Measured October 2001	Measured January 2003	Measured January 2003
Cs	360.9	41.64	39.70	41.46	39.45	40.12	41.45	41.15
Rb	431.1	31.63	30.69	32.75	30.42	33.28	32.92	31.67
Ba	424.1	37.74	36.76	36.75	35.91	33.42	38.76	37.94
Th	450.6	37.23	37.06	35.03	34.93	34.91	36.81	37.42
U	457.1	37.15	34.88	34.84	38.01	36.71	36.35	34.05
Nb	419.4	38.06	35.16	36.65	33.55	33.48	35.88	36.47
Ta	376.6	39.77	30.06	30.27	29.99	30.68	30.27	32.30
La	457.4	35.77	37.80	37.30	35.35	35.23	37.30	37.24
Ce	447.8	38.35	37.16	38.23	36.76	37.16	37.72	39.05
Pb	413.3	38.96	33.37	33.24	37.37	38.64	35.81	35.33
Pr	429.8	37.16	35.97	36.70	34.85	34.60	35.28	35.51
Sr	497.4	76.15	78.39	79.89	75.23	75.22	76.17	79.57
Nd	430.8	35.24	35.08	35.26	34.67	32.25	34.37	35.87
Zr	439.9	35.99	38.60	39.60	36.10	35.80	38.34	40.05
Hf	417.7	34.77	35.47	34.79	34.47	34.27	33.88	34.29
Sm	450.5	36.72	37.97	37.29	34.36	34.62	35.88	36.44
Eu	461.1	34.44	36.16	37.30	35.29	34.35	37.05	37.41
Sn	396.3	37.96	35.11	37.32	35.05	34.72	36.71	34.61
Gd	419.9	36.95	34.13	35.50	33.55	32.66	34.01	36.62
Tb	442.8	35.92	36.09	37.38	35.63	34.08	34.83	37.04
Dy	426.5	35.97	34.51	33.62	33.21	31.87	33.20	37.38
Li	484.6	41.54	41.95	39.87	40.88	42.35	42.64	42.56
Y	449.9	38.25	38.57	38.96	35.70	34.60	36.90	38.50
Ho	449.4	37.87	37.21	38.46	34.85	35.14	36.14	37.54
Er	426.0	37.43	36.72	37.37	34.01	35.64	35.85	37.81
Tm	420.1	37.55	35.74	35.30	33.23	34.10	34.81	37.34
Yb	461.5	39.95	38.39	39.43	35.89	35.57	38.54	39.81
Lu	434.7	37.71	37.13	35.79	34.05	34.45	36.12	38.06
Sc	441.1	41.05	42.37	41.95	35.97	35.84	39.14	42.33
V	441.7	39.22	37.74	39.97	39.04	38.33	39.29	36.59
Co	405.0	35.26	34.40	37.10	35.63	35.29	34.40	34.48
Zn	456.3	37.92	37.99	39.95	40.62	40.55	37.69	39.52
Ga	438.1	36.24	36.64	38.97	37.72	38.57	39.36	36.91

repeated analyses of standards, is approximately ±5% for element concentrations >10 ppm and ±10% for concentrations <10 ppm. Data processing was carried out offline using the same PlasmaLab software used for data collection and various custom-designed Excel spreadsheets. The limits of detection are defined as 3.28 standard deviations above background level, which equates to a 95% confidence that the measured signal is significantly above background. Typical detection limits are 1–20 ppm for Sc, V, Co, Cu, Zn, Ga, Rb and Ba, 0.2–1 ppm for Sr, Y, Zr, Nb, Sn, Cs, Hf and Pb and 0.05–0.6 ppm for the REE, U, Th and Ta. Detection limits for Li are highly variable between 2 and 80 ppm depending on the specific setting during measurements.

The major and minor element composition of minerals was determined using a JEOL 8900 electron microprobe at the Institut für Geowissenschaften at the Universität Tübingen, Germany. Both natural and synthetic standards were used for calibration. The beam current was 15 nA and the acceleration voltage was 15 kV. The counting time on the peak was 16 s for major elements and 30–60 s for minor elements (Mn, Ti, Zr, F, Cl). Background counting times were half peak counting times. The peak overlap between the Fe Lβ and F Kα lines was corrected for. Data reduction was performed using the internal ϕρZ procedures of JEOL (Armstrong, 1991).

4. Major element compositional trends of clinopyroxene and amphibole from the three investigated complexes

4.1. Clinopyroxene

The pyroxene trends observed in the three investigated intrusive complexes are shown in Fig. 2a. In all three complexes, the most primitive pyroxenes (in terms of X_{Fe}) are diopsidic with low Na contents (<0.1 apfu). During fractionation, pyroxene composition gets more Fe- and Na-rich, reaching almost end-member aegirine composition in Puklen and Ilímaussaq (Larsen, 1976; Marks and Markl, 2001; Markl et al., 2001b; Marks et al., 2003). Differences in the degree and timing of Na- and Fe^{3+}-enrichment can be attributed to oxygen fugacity during crystallization: the strongly reducing conditions (below the FMQ buffer) in the Ilímaussaq complex and in most of the Puklen samples allow a strong Fe-enrichment, but still low Na contents during fractionation (e.g., Larsen, 1976). In contrast, more oxidized conditions in the Grønnedal-Ika complex (Pearce et al., 1997a,b; Halama et al., in press) result in relatively high Na- and Fe^{3+}-contents at intermediate Fe/Mg ratios. A similar compositional trend found in the Puklen complex is the result of more oxidized (ΔFMQ=+1) conditions during late-magmatic autometasomatism (Marks et al., 2003).

4.2. Amphibole

Fig. 2b shows the amphibole trends observed in the three investigated intrusive complexes in the Ca_B vs. Si diagram after Mitchell (1990). The Puklen and Ilímaussaq trends are typical for alkaline to peralkaline igneous rocks. Primary amphibole ranges in composition from almost pure Ca-amphibole (ferro-edenite, ferro-pargasite, hastingsite) with relatively high Al-contents in the early rock types and evolves via Na–Ca amphibole (katophorite, ferro-richterite) to Na-amphibole (nyböite, arfvedsonite, leakeite) in the most evolved rocks. Secondary amphibole in the Puklen rocks evolves from ferro-edenite towards ferro-actinolite, which is known only from silica-oversaturated alkaline complexes (Mitchell, 1990). Amphiboles in the Grønnedal-Ika syenites are mainly sodic–calcic katophorites; sodic and calcic amphiboles are very scarce (Bedford, 1989).

5. Trace element compositions

Overall, more than 230 trace element analyses of clinopyroxene and 150 analyses of amphibole were performed. In order to present a good overview of the whole data set, we present the averages of analyses from the respective minerals of each sample studied. In cases of significant chemical zoning with respect to major and trace element composition within individual grains, representative zoning profiles are shown. Typical analyses of clinopyroxene and amphibole from the three investigated igneous complexes are summarized in Tables 3 and 4. All rare earth element

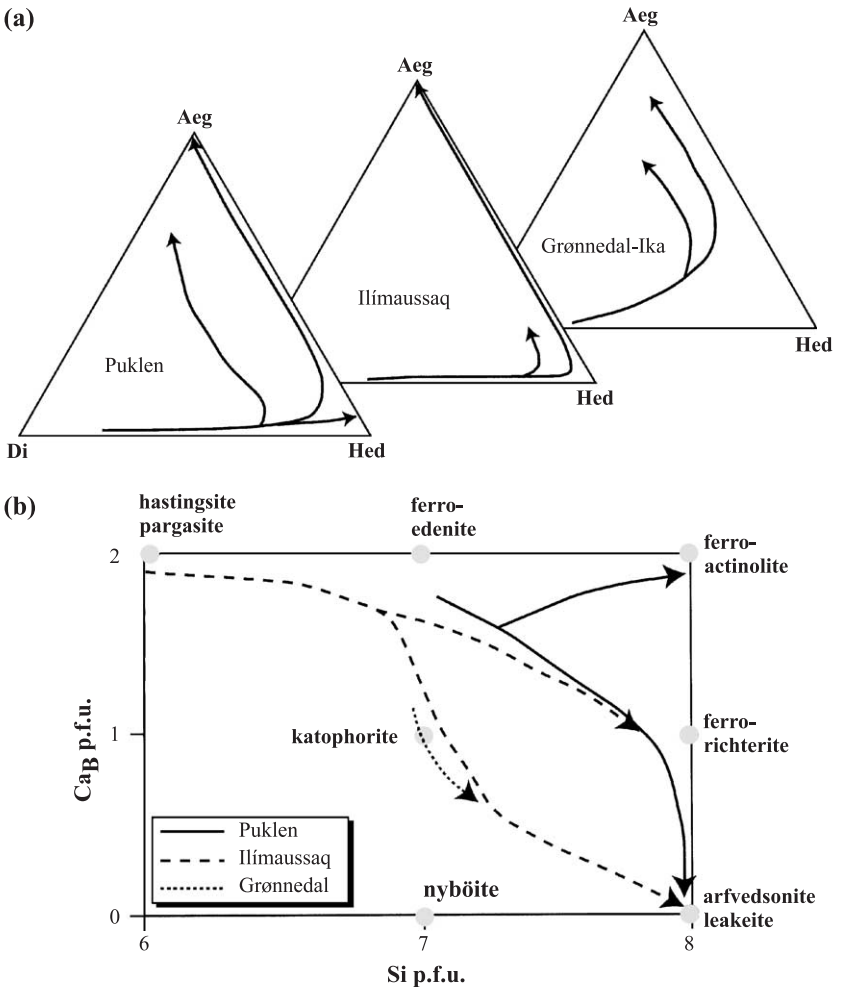

Fig. 2. (a) Major element compositional trends for clinopyroxenes of the three complexes studied, after data from Larsen (1976), Marks and Markl (2001), Markl et al. (2001b), Marks et al. (2003) and Halama et al. (in press). (b) Major element compositional trends for amphiboles of the three complexes studied, after data from Larsen (1976), Marks et al. (2004), Marks et al. (2003) and Halama et al. (in press).

(REE) and trace element (TE) patterns are normalized to the primitive mantle values of McDonough and Sun (1995). The order of presentation for both clinopyroxenes and amphiboles follows the above-described major element trends starting with the Ca-rich end members.

5.1. Clinopyroxene

5.1.1. Augites of Puklen and Ilímaussaq

Fig. 3a and b shows average REE and TE patterns from augites of Puklen and Ilímaussaq, which are characterized by low Na/Ca ratios <0.15. Normalized REE concentrations for all augites are 10 to 200 times enriched relative to primitive mantle values. The patterns are sinusoidal and show strongly developed negative Eu anomalies (Eu/Eu*=0.12–0.38 for Puklen and 0.31 and 0.42 for Ilímaussaq). La_N/Yb_N values vary between 1.5 and 3.7 (Puklen) and between 2.1 and 2.3 (Ilímaussaq).

Most other incompatible elements are enriched by a factor of about 10 to 100 compared to primitive mantle values. For all augites, relative depletions for the HFSE (Ti, Zr, Hf, Nb) can be detected. For the large ion lithophile elements (LILE), strong negative peaks are observed for Ba and Sr and also for Pb

Table 3
Average major, minor and trace element contents of clinopyroxenes from Ilímaussaq, Puklen and Grønnedal-Ika

Complex	Ilímaussaq	Puklen	Puklen	Grønnedal-Ika	Grønnedal-Ika	Grønnedal-Ika	Grønnedal-Ika	Ilímaussaq	Ilímaussaq	Ilímaussaq	Puklen	Puklen
Rock type	Augite syenite	Syenite	Syenite	Nepheline syenite	Nepheline syenite	Nepheline syenite	Nepheline syenite	Alkali granite	Agpaite	Agpaite	Alkali granite	Microgranite
Sample no.	GM1331	GM 1586	GM1600	GR44	GM1526	GM1496	GM1496	GM1303	GM1294	GM1334	GM1587	GM1620
Clinopyroxene type	Augite	Augite	Augite	Aegirine–augite	Aegirine–augite	Aegirine–augite core	Aegirine–augite rim	Aegirine	Aegirine	Aegirine	Aegirine	Aegirine
No. of analyses	6	14	8	10	10	3	2	8	4	7	8	11
Major and minor elements (wt.%)[a]												
SiO_2	50.35	49.53	50.27	50.77	51.80	50.29	51.11	51.89	52.45	52.88	52.48	53.06
TiO_2	0.91	0.61	0.95	0.20	0.16	0.35	0.32	0.56	0.69	0.59	0.93	0.37
Al_2O_3	1.73	0.53	0.80	1.14	0.99	2.50	1.07	0.13	1.33	1.07	0.31	0.28
FeO	14.17	24.53	20.27	21.53	24.54	17.35	21.45	30.46	28.72	28.24	30.38	27.36
MnO	0.49	0.66	0.50	0.90	0.78	0.38	0.67	0.08	0.08	0.12	0.18	0.56
MgO	10.55	3.46	6.36	4.35	2.08	6.75	3.91	0.08	0.01	0.13	0.04	1.35
CaO	21.06	19.75	19.71	17.93	11.56	19.41	14.05	0.08	0.54	2.27	0.09	4.38
Na_2O	0.53	0.82	0.93	3.30	7.17	2.22	5.68	13.14	13.46	12.41	13.35	11.73
K_2O	0.01	0.02	0.01	0.00	0.01	0.01	0.05	0.01	0.00	0.02	0.04	0.01
Total	99.81	99.92	99.80	100.12	99.09	99.26	98.32	96.43	97.28	97.73	97.79	99.09
Na/Ca ratio	0.05	0.08	0.08	0.33	1.12	0.21	0.73	297	45	9.9	275	4.8
X_{Fe}	0.43	0.79	0.62	0.64	0.72	0.52	0.57	0.97	1.00	0.91	0.99	0.51
Trace elements (ppm)												
Cs	0.15	0.63	0.95	-	0.25	-	-	0.31	0.20	0.18	13.1	0.01
Rb	0.85	3.31	6.41	2.49	2.11	3.06	1.18	0.77	0.68	1.04	107	6.60
Ba	1.14	2.14	21.6	0.85	1.89	1.53	-	3.26	0.49	0.37	175	2.52
Th	0.98	0.26	4.90	0.29	0.19	-	0.10	1.19	0.49	0.14	15.8	0.35

U	0.44	0.36	1.62	0.08	0.08	0.04	-	0.46	0.14	0.05	14.5	0.23
Nb	1.01	0.79	8.23	2.96	9.02	2.40	3.69	27.0	74.9	4.67	371	48.0
Ta	n.a.	0.14	1.68	0.48	0.91	0.23	0.87	1.43	n.a.	n.a.	22.7	1.69
La	28.91	32.44	13.4	43.4	11.2	8.17	9.73	2.41	4.06	5.01	370	39.5
Ce	104.4	98.11	313	140	42.8	32.5	38.9	7.17	11.4	13.8	622	115
Pb	0.74	1.71	35.6	0.49	0.46	0.21	0.27	25.0	28.8	0.82	1172	2.20
Pr	16.45	17.54	45.6	22.9	8.19	5.90	7.60	1.17	1.82	1.97	76.6	18.2
Sr	27.65	5.80	43.2	205	56.9	589	352	2.01	2.44	4.62	38.0	6.50
Nd	75.81	92.74	219	106	41.2	33.5	41.6	5.72	7.89	8.38	368	86.5
Zr	243.1	199.1	90.3	1127	5721	127	6218	1338	982	1406	2303	234
Hf	7.26	6.74	3.98	29.4	145	3.01	116.1	54.2	18.7	29.0	51.1	7.52
Sm	19.42	23.32	53.0	23.1	10.4	9.13	12.5	3.43	1.83	1.48	76.1	19.5
Eu	2.35	1.72	1.93	4.80	2.03	3.48	3.28	0.20	0.20	0.15	3.99	0.99
Sn	1.43	1.95	4.64	8.11	54.7	1.32	45.3	97.3	265	169	125	2.06
Gd	14.97	19.69	44.8	15.6	6.81	7.09	7.29	4.08	1.59	0.99	77.0	15.0
Tb	2.62	3.15	7.63	2.12	1.26	0.94	1.14	1.14	0.30	0.15	11.7	2.48
Dy	15.16	17.67	45.9	11.5	6.91	4.65	7.19	9.11	1.61	0.92	60.3	15.2
Li	32.0	195.0	278	8.47	5.31	8.76	2.49	71.0	25.0	29.0	148	176
Y	68.90	84.57	228	42.9	23.4	13.8	24.3	35.5	7.62	4.38	429	78.0
Ho	3.03	3.70	9.11	1.97	1.37	0.61	1.44	2.47	0.27	0.21	13.4	3.18
Er	7.87	9.52	23.9	5.62	4.76	1.32	4.49	10.4	0.79	0.77	39.0	10.8
Tm	1.17	1.64	3.40	1.03	1.15	0.16	0.84	2.02	0.20	0.24	6.03	1.88
Yb	8.87	14.84	23.4	9.16	13.5	0.80	8.96	11.5	2.13	3.08	45.4	18.0
Lu	1.40	2.83	3.69	1.88	2.78	0.15	2.06	1.77	0.51	0.79	6.53	3.45
Sc	210.3	121.2	118	12.8	13.2	8.50	2.45	2.44	3.44	10.6	7.38	53.0
V	3.99	1.38	196	12.1	4.21	148	8.99	0.76	0.20	5.73	8.41	3.50
Co	n.a.	10.60	111	12.3	6.59	22.8	7.85	n.a.	n.a.	n.a.	7.90	5.31
Zn	199.9	276.4	487	247	306	89.2	322	376	61.6	130	1033	385
Ga	10.63	6.40	7.56	10.5	12.8	12.1	19.3	5.66	72.2	40.6	13.7	4.60

n.a.=not analyzed.

−=not detected.

[a] Analyzed by electron microprobe.

Table 4
Average major, minor and trace element contents of amphiboles from Ilímaussaq, Puklen and Grønnedal-Ika

Complex	Ilímaussaq	Puklen	Puklen	Puklen	Puklen	Grønnedal-Ika	Ilímaussaq	Ilímaussaq	Puklen	Puklen
Rock type	Augite syenite	Granophyre	Syenite	Granophyre	Syenite	Nepheline syenite	Alkali granite	Agpaite	Alkali granite	Microgranite
Sample no.	GM1331	GM1593	GM1600	GM1593	GM1615	GM1526	GM1303	GM1334	GM1587	GM1620
Amphibole type	Calcic ferro-pargasite	Calcic I ferro-edenite	Calcic I ferro-edenite	Calcic II ferro-actinolite	Sodic–calcic ferro-richterite	Sodic–calcic katophorite	Sodic arfvedsonite	Sodic arfvedsonite	Sodic arfvedsonite	Sodic arfvedsonite
No. of analyses	6	8	9	4	7	1	14	7	7	5
Major and minor elements (wt.%)[a]										
SiO_2	41.07	44.08	44.98	50.42	48.67	44.55	43.66	47.39	51.07	49.59
TiO_2	3.13	0.83	1.25	0.06	1.10	1.12	1.10	0.73	1.92	0.69
Al_2O_3	9.04	5.00	5.00	0.74	0.82	5.65	5.53	2.96	0.53	2.38
FeO	19.42	29.51	28.04	33.42	31.53	27.59	27.04	33.17	29.90	29.36
MnO	0.38	0.34	0.53	0.41	0.74	1.10	1.08	0.66	0.84	0.78
MgO	8.90	4.03	5.09	2.45	0.62	4.18	4.10	0.84	1.14	3.84
CaO	10.55	9.62	9.54	10.54	5.60	6.47	6.34	2.38	0.24	5.21
Na_2O	2.71	2.86	2.61	0.85	6.08	5.37	5.26	7.71	8.61	5.44
K_2O	1.49	0.99	0.91	0.26	1.27	1.72	1.68	1.74	1.58	0.56
Cl	0.13	0.30	0.26	0.01	0.04	0.03	0.03	0.00	0.02	0.14
F	0.72	1.57	2.33	0.00	0.74	1.13	1.11	0.07	2.57	0.13
Total	97.55	99.13	100.55	99.16	97.23	98.91	96.94	97.66	98.42	98.13
Na/Ca ratio	0.46	0.54	0.50	0.15	1.95	1.50	44.65	5.88	65.56	1.87
X_{Fe}	0.55	0.80	0.76	0.88	0.96	0.75	1.00	0.94	0.92	0.81
Trace elements (ppm)										
Cs	0.02	1.43	1.01	–	0.39	–	–	0.20	14.8	0.69
Rb	19.4	105	12.3	–	28.9	18.7	53.4	41.3	192	13.2
Ba	303	161	13.5	2.90	2.85	3.37	1.20	3.18	79.5	2.17
Th	23.3	4.31	2.40	3.05	0.35	–	1.48	0.20	154	1.65
U	6.61	1.00	0.24	0.32	0.14	–	1.33	0.13	9.84	0.93

Nb	365	303	86.5	10.4	137	517	94.6	132.8	355	36.4
Ta	n.a.	7.57	1.93	0.88	2.11	20.4	1.22	n.a.	11.0	1.06
La	253	72.4	109	32.5	42.0	53.9	12.4	17.9	3986	104
Ce	557	264	407	57.9	103	145	44.2	44.1	7791	300
Pb	5.89	28.5	20.0	9.39	7.41	0.95	15.0	2.55	1260	24.0
Pr	168	37.1	57.8	7.47	15.0	20.1	4.74	5.67	1169	41.1
Sr	96.6	30.4	25.1	10.7	15.3	93.7	5.99	18.9	726	37.4
Nd	692	155	245	28.7	66.7	84.1	17.3	21.3	4993	186
Zr	1640	50.9	976	52.6	1087	1766	853	1472	1697	576
Hf	49.9	2.92	8.18	4.91	25.4	50.4	27.2	34.2	39.3	15.5
Sm	134	39.6	61.6	6.11	12.6	15.4	2.98	3.00	771	62.2
Eu	9.65	0.70	1.68	0.37	0.88	2.56	0.23	1.00	36.0	3.00
Sn	4.50	96.2	14.6	41.8	9.56	19.1	38.1	39.1	58.9	20.8
Gd	95.4	30.7	46.3	5.67	9.03	7.79	1.83	1.50	612	43.5
Tb	14.0	6.45	8.38	1.11	1.72	1.16	0.41	0.51	86.6	6.50
Dy	76.1	42.8	50.3	7.21	14.2	5.47	3.72	1.90	505	41.6
Li	29.0	722	167	240	1466	31.3	756	390	2895	288
Y	345	250	269	48.5	130	18.4	21.6	12.1	2494	177
Ho	14.7	9.28	10.0	1.64	4.87	0.92	1.49	0.73	122	9.51
Er	36.7	25.7	26.2	5.95	24.6	2.70	8.77	2.49	298	23.6
Tm	4.89	4.12	3.83	1.63	6.67	0.53	2.78	0.78	33.7	4.11
Yb	32.4	31.1	29.9	22.7	65.3	5.17	35.3	8.04	191	38.6
Lu	4.38	4.36	4.39	5.81	13.1	1.04	7.88	1.58	26.1	7.77
Sc	156	83.6	54.6	40.4	48.4	6.44	8.43	11.7	20.8	42.0
V	1.64	29.0	147	5.77	4.75	1.41	0.89	7.32	32.6	4.20
Co	n.a.	43.6	29.8	n.a.	17.6	19.8	3.23	n.a.	13.0	8.80
Zn	381	1381	1109	1927	1476	592	3287	956	4667	931
Ga	56.0	45.5	23.5	5.32	13.2	32.3	6.16	36.0	16.2	6.40

n.a.=not analyzed.

−=not detected.

[a] Analyzed by electron microprobe.

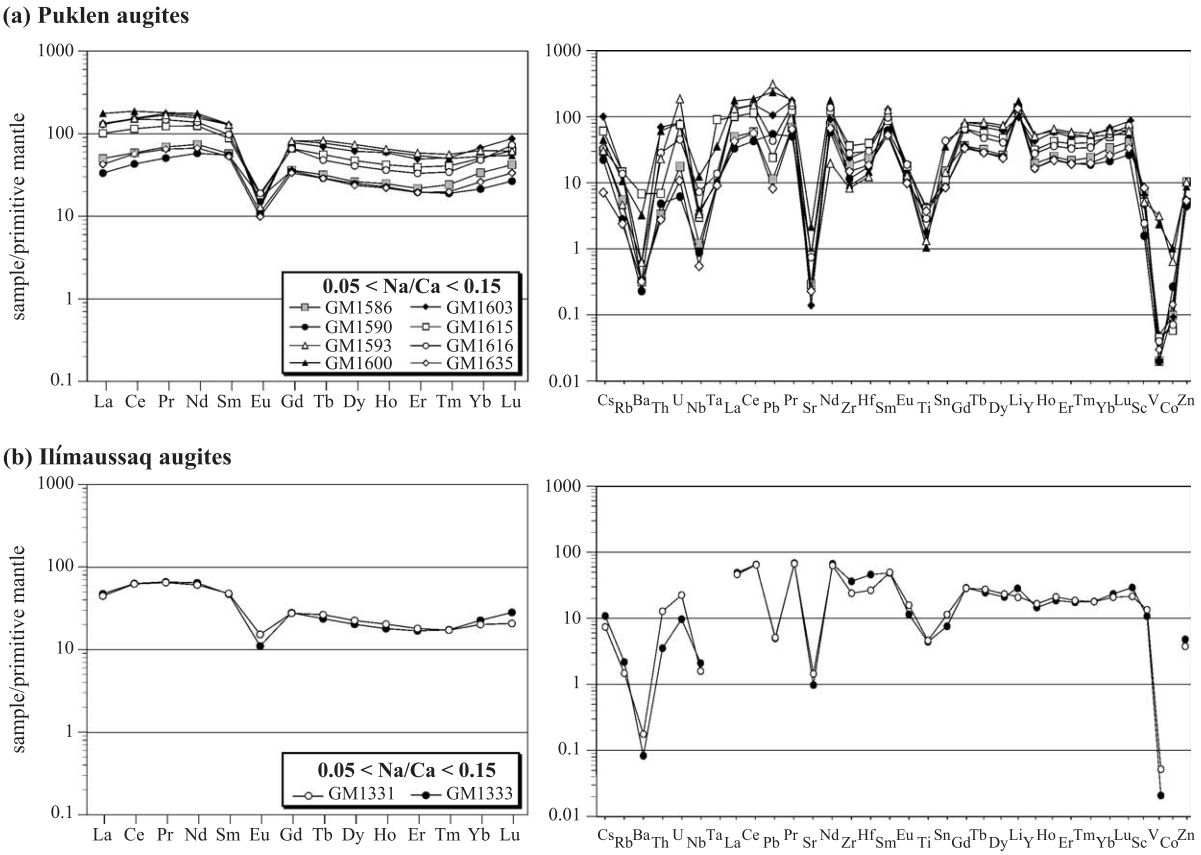

Fig. 3. Averaged primitive mantle-normalized REE and TE patterns for augites of (a) Puklen and (b) Ilímaussaq. Normalizing values are after McDonough and Sun (1995).

except for three Puklen samples. The transitional metals Sc, V, Co and Zn are generally less enriched (Sc and Zn) or even depleted (V and Co). Principally, the REE and TE patterns for augites from Puklen and Ilímaussaq are very similar. However, the negative peaks for Pb and Sr are stronger developed in the Ilímaussaq augites whereas those of Zr, Hf and Ti appear to be weaker than in Puklen augites. In augites from Puklen, a slightly positive anomaly of Li can be detected, which is less pronounced in the Ilímaussaq augites.

Fig. 4 shows representative zoning profiles (Na p.f.u., X_{Fe} and selected trace element contents) across an augite from Puklen (Fig. 4a) and Ilímaussaq (Fig. 4b), respectively. Both profiles show similar characteristics. With increasing fractionation (increase of X_{Fe} and Na content from core to rim), Sc decreases, and Zn, Zr and the REE increase. Whereas the amount of enrichment of Zn is more or less equal in both augites, the enrichment of Zr and REE_{tot} is much more extensive in the Ilímaussaq than in the Puklen augite.

5.1.2. Aegirine–augites of Grønnedal-Ika

REE and TE patterns for aegirine–augites of Grønnedal-Ika are shown in Fig. 5. Their Na/Ca ratios vary between 0.2 and 2. The enrichment levels for REE and most other TE are in a similar range compared to augites. Besides the lack of a significant Eu anomaly (Eu/Eu*=0.69–1.16) and stronger enrichment in Tm–Lu, the shape of the REE patterns is rather similar to that of augites (Fig. 5a). La_N/Yb_N ratios are quite variable with a range from 0.6 to 6.5.

As for augites, negative peaks are detected for some LILE (Ba, Pb, Sr), Ti and the transitional

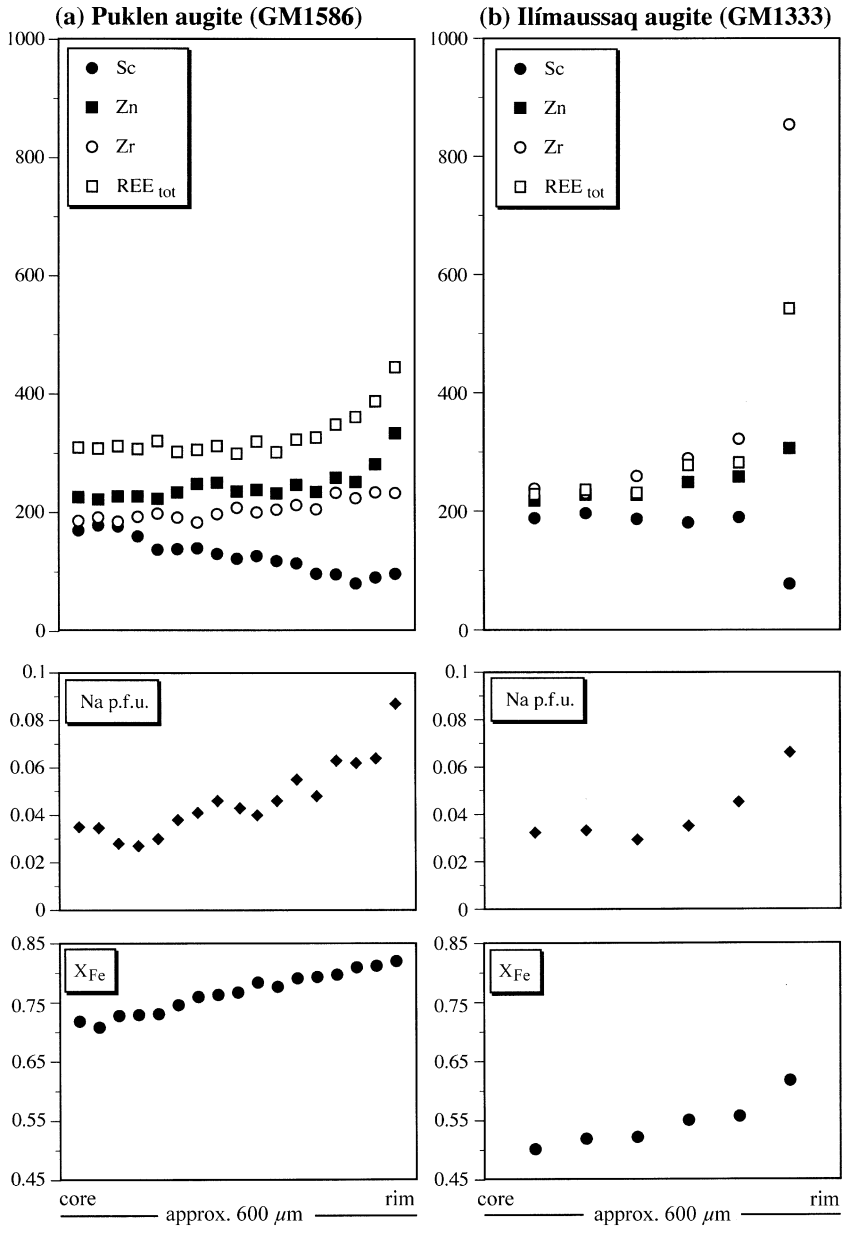

Fig. 4. Zoning profiles for selected elements and X_{Fe} from core to rim of augite from (a) Puklen and (b) Ilímaussaq.

elements (Sc, V, Co). In contrast to augites, positive peaks for Zr, Hf and Sn, and a negative Li anomaly are developed.

In most samples, aegirine–augites are fairly homogeneous. However, in one sample (GM1496), aegirine–augite with a relatively low Na/Ca ratio of about 0.2 shows a thin rim of distinctly more Na-rich compositions (Na/Ca ratio ~0.7). Mantle-normalized REE patterns and TE patterns of core and rim compositions for a typical crystal of this sample are shown in Fig. 5b. The core pattern is parallel to that of the rim from La to Gd but shows a strong decrease towards Lu. Furthermore, rim compositions are enriched in Zr, Hf, Sn and Zn but depleted in Li,

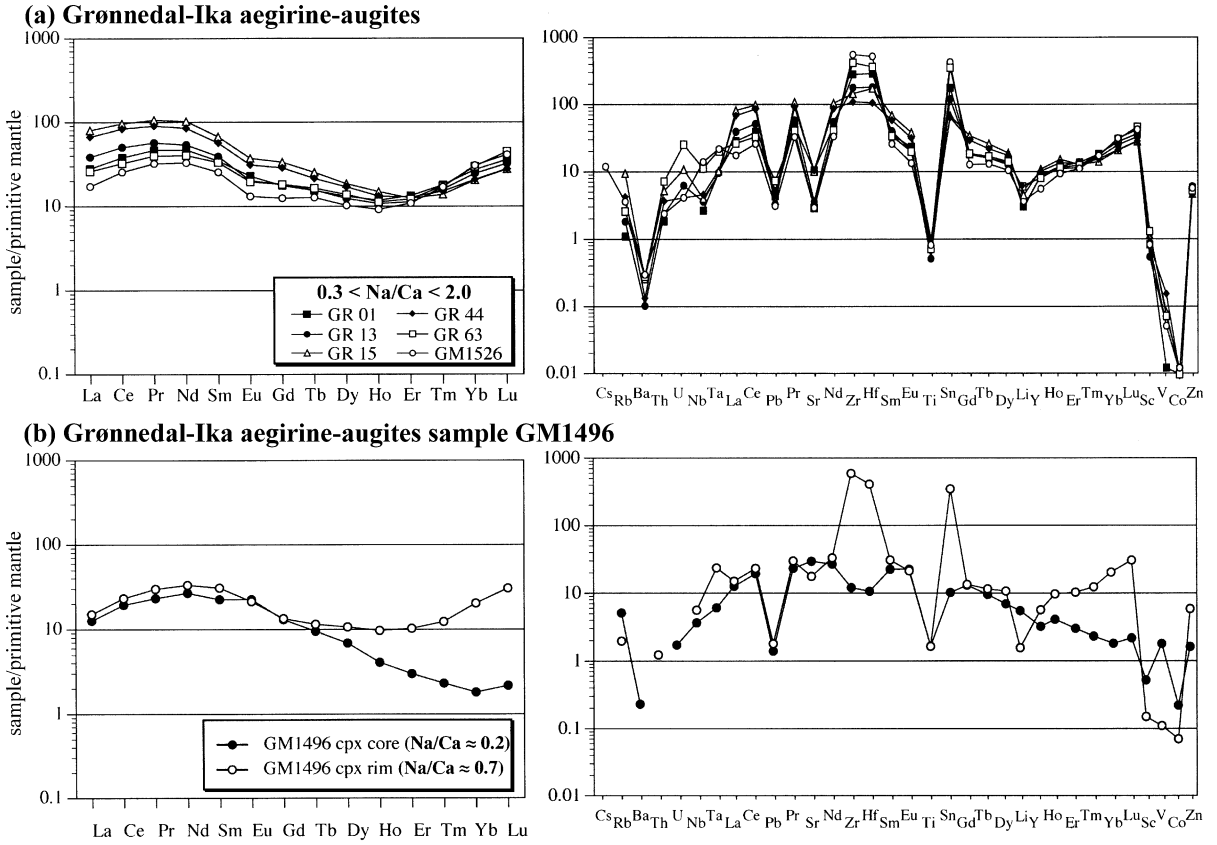

Fig. 5. (a) Averaged mantle-normalized REE and TE patterns for aegirine–augites of Grønnedal. (b) Mantle-normalized REE patterns and TE patterns of core and rim compositions for an individual aegirine–augite of sample GM1496.

Sc, V and Co compared to the core and are generally similar to the patterns of the other aegirine–augites (Fig. 5a).

5.1.3. Aegirines of Puklen and Ilímaussaq

Average mantle-normalized REE patterns for aegirines (Fig. 6) are variable in their level of enrichment, their extent of negative Eu anomalies (Eu/Eu*=0.16–0.63) and their shape, especially for the Puklen aegirines. With the exception of one sample, all Puklen aegirines show a more or less pronounced enrichment of HREE, whereas all Ilímaussaq aegirines are enriched in both LREE and HREE. This results in a V-shaped pattern, which seems to be typical of aegirines (Larsen, 1976; Shearer and Larsen, 1994; Piilonen et al., 1998). La_N/Yb_N ratios are typically lower than in augites and aegirine–augites and vary from 0.1 to 2.9.

As for augites and aegirine–augites, multi-element diagrams for aegirines show more or less pronounced negative peaks for Ba, Sr, V and Co (Fig. 6). In contrast, normalized Pb concentrations are variable with some aegirines having a clear positive and some a slightly negative Pb peak. As in aegirine–augites, positive peaks for Zr, Hf and Sn are present, whereas the negative Ti peak has disappeared in the aegirines. A positive Li anomaly can be found in most aegirines similar to most augites, but unlike the aegirine–augites.

5.2. Amphibole

5.2.1. Ca and Na–Ca-amphiboles of Puklen, Ilímaussaq and Grønnedal-Ika

Average REE patterns of Ca- and Ca–Na-amphiboles are shown in Figs. 7 and 8. The Puklen

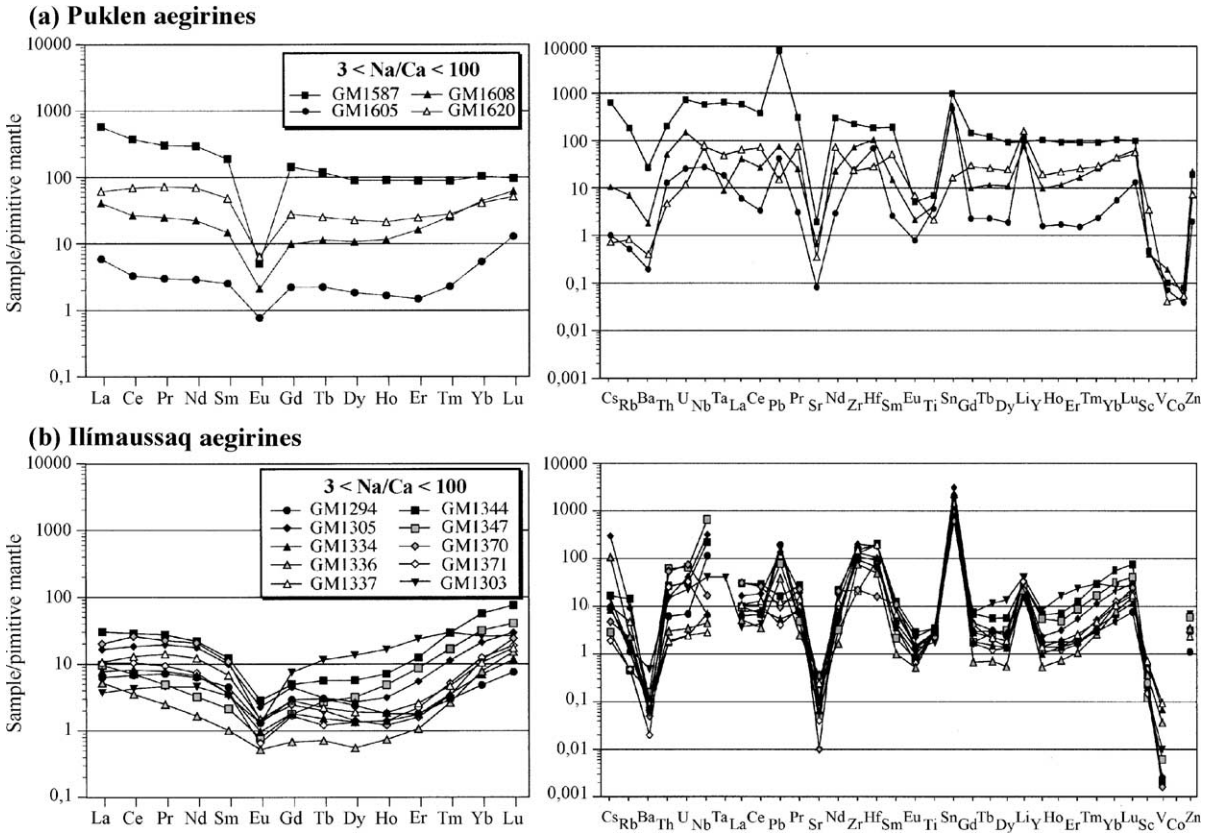

Fig. 6. Averaged mantle-normalized REE and TE patterns for aegirines of (a) Puklen and (b) Ilímaussaq.

amphiboles have strongly developed negative Eu anomalies (Eu/Eu*=0.06–0.29), but two different patterns can be distinguished: Ferro-richterites show pronounced HREE-enrichment with La_N/Yb_N ratios between 0.47 and 0.45. In contrast, variably developed LREE-enrichment and a flat HREE section resulting in La_N/Yb_N ratios between 1.5 and 2.5 characterize ferro-edenites. Secondary ferro-actinolites from Puklen syenites are heterogeneous in terms of enrichment level and shape with La_N/Yb_N ratios between 0.7 and 1.1. REE patterns of Ilímaussaq ferro-pargasites from the augite syenite are characterized by significant negative Eu-anomalies (Eu/Eu*=0.26 and 0.30), a LREE enrichment and a smooth decrease from Gd to Lu. La_N/Yb_N ratios vary from 5.3 to 8.6. The Grønnedal-Ika katophorites lack a significant Eu anomaly (Eu/Eu*=0.70–0.71). They show slight enrichments in LREE and the heaviest REE (La_N/Yb_N=4.4 and 7.1).

Most trace elements in Ca- and Ca–Na amphiboles are 5–300 times enriched compared to primitive mantle values. Characteristic features of most samples are negative anomalies for Ba, Sr, V and Co and positive ones for Sn and Li. Strong negative Pb anomalies are only present in amphiboles from Ilímaussaq and Grønnedal-Ika. Positive Zr-Hf peaks do not occur in the Ca-amphiboles, but in the Ca–Na amphiboles of Grønnedal-Ika.

Fig. 9 shows a representative zoning profile from core to rim of a Ca–Na amphibole crystal from a Puklen syenite (GM1615). The contents of Zr, Zn and REE increase from core to rim. With increasing fractionation (increase in X_{Fe} and Na/Ca ratio), LREE (La as example) slightly decrease and HREE (Yb as example) strongly increase resulting in a decrease of the La_N/Yb_N ratio from about 1.2–1.3 in the core regions to about 0.13 at the rim of crystals. However, the Eu/Eu* value remains relatively constant at about 0.25.

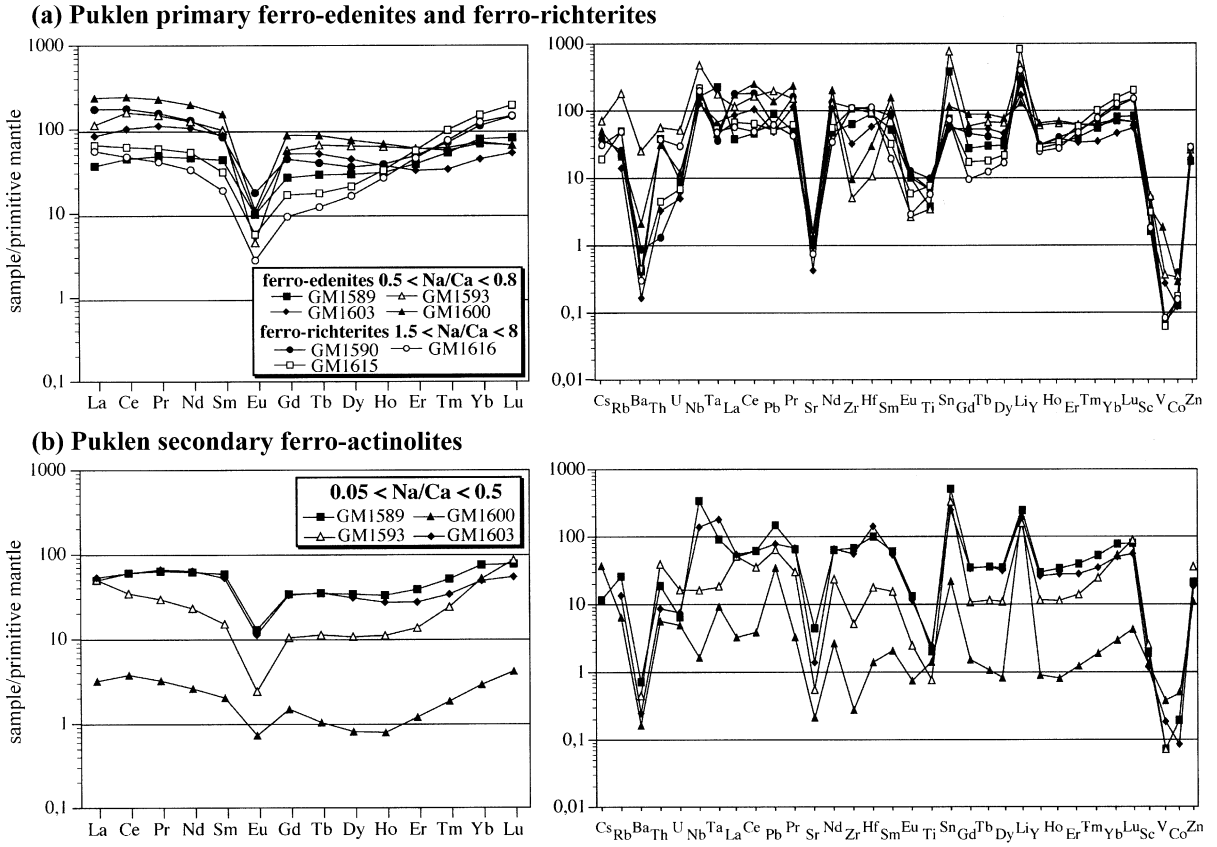

Fig. 7. Averaged mantle-normalized REE and TE patterns for (a) ferro-edenites and ferro-richterites and (b) ferro-actinolites of Puklen.

5.2.2. Na-amphiboles of Puklen and Ilímaussaq

REE and TE spectra of arfvedsonites are shown in Fig. 10. Eu anomalies are strongly negative in the Puklen arfvedsonites (Eu/Eu*=0.04 and 0.19), but more variable in Ilímaussaq arfvedsonites (Eu/Eu*=0.26–0.92). The enrichment of LREE and HREE is highly variable developed with La_N/Yb_N ratios <1 to 4. TE patterns of arfvedsonites are highly heterogeneous within and among the Puklen and Ilímaussaq rocks. Highly variable concentrations can be observed for Th, U, Pb, Zr and Hf. Most Ilímaussaq Na-amphiboles have positive anomalies of Zr, Hf, Nb, Sn and Li, which are much less prominent in Puklen.

Principally, zoning profiles of arfvedsonite from Puklen and Ilímaussaq (Fig. 11) show similar characteristics as the profiles of Ca-amphiboles (Fig. 9) and augites (Fig. 4), except for the REE. Zn and Zr increase from core to rim and Sc decreases. However, the total content of REE decreases with fractionation, which is in contrast to the behavior of augites and Ca-amphiboles. The behavior of LREE and HREE in the two amphibole types is different: in Na-amphiboles, LREE and HREE have similar concentrations in the core regions. During fractionation, HREE contents remain fairly constant, whereas LREE concentrations strongly decrease. This is in contrast to Ca-amphiboles, where LREE contents slightly decrease and HREE strongly increase during fractionation. Both processes result in a decrease of the La_N/Yb_N ratio with increasing fractionation.

6. Discussion

In principle, relative trace element abundances in minerals can reflect the influence of two factors: First, the composition and structure of the melts or fluid phases they crystallized from (e.g., Adam and Green,

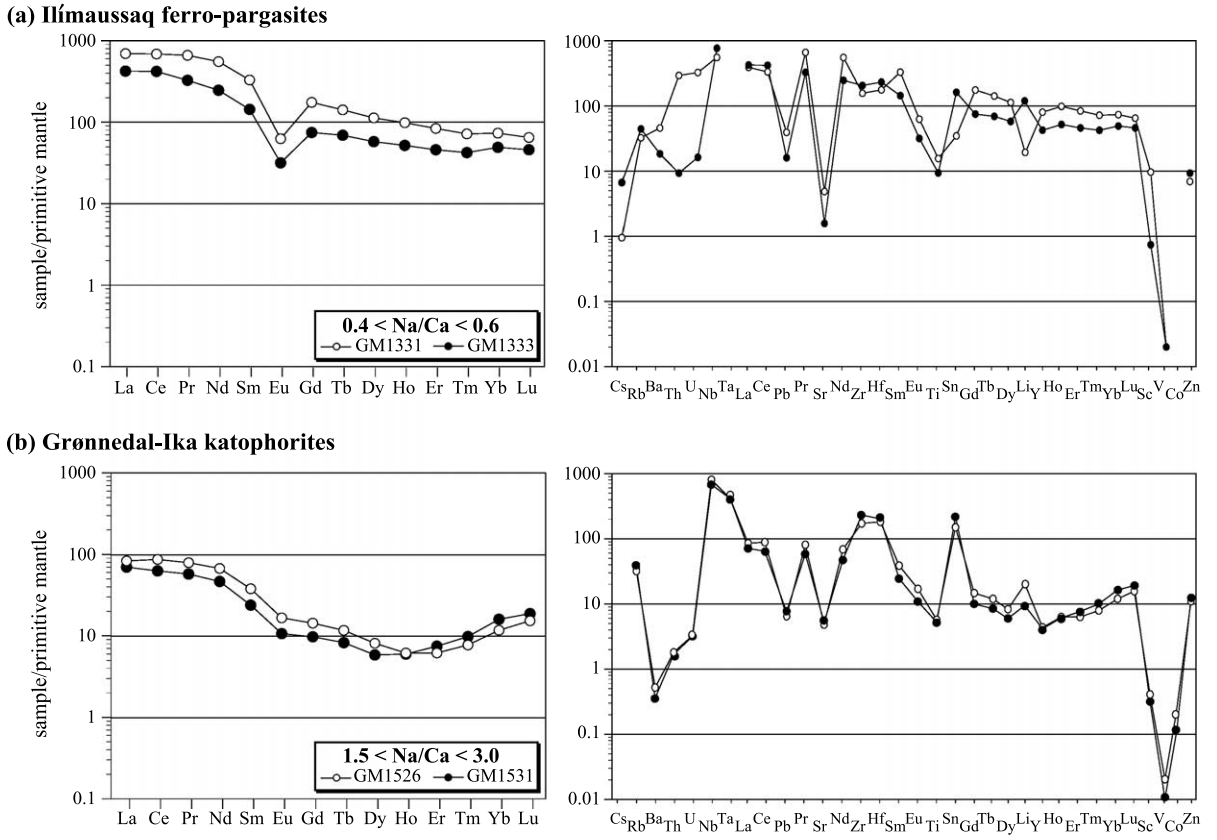

Fig. 8. Averaged mantle-normalized REE and TE patterns for (a) ferro-pargasites of Ilímaussaq and (b) katophorites of Grønnedal.

2003; Bennett et al., 2003), and, second, the control by crystal-chemical effects (e.g., Blundy and Wood, 1994). The latter implies that the major element composition of the crystals dominates the incorporation of the trace elements (e.g., Blundy and Wood, 1991; Wood and Blundy, 1997). Additional parameters that influence trace element partitioning to a lesser extent are P, T and f_{O2}.

Absolute trace-element abundances in melts may depend on the fractionation of minerals that preferentially incorporate certain trace elements and on assimilation of crustal material. In the Gardar Province, early plagioclase fractionation is indicated by the abundant occurrence of anorthosite xenoliths (Bridgwater, 1967; Bridgwater and Harry, 1968; Halama et al., 2002) and negative Eu anomalies in whole-rock samples of the Ilímaussaq complex (Bailey et al., 2001). Furthermore, fractionation of alkali feldspar is seen in the investigated complexes. Since negative Eu anomalies are mostly controlled by feldspar fractionation (Drake and Weill, 1975), and Ba, Sr, Eu^{2+} and, to a lesser extent, Pb are compatible in alkali feldspar in silicic magmas (Nash and Crecraft, 1985; White, 2003), the absolute concentrations of these are likely to be generally diminished in the residual Gardar magmas from which the complexes crystallized. The lack of significant negative Eu anomalies in the Grønnedal-Ika samples is probably related to the more oxidized conditions (Bedford, 1989; Pearce et al., 1997a) leading to the stabilization of Eu^{3+}, which is incompatible in feldspar. Low concentrations of Co and V in the investigated mafic minerals might be attributed to early precipitation of olivine and spinel because both are compatible in olivine and/or spinel (Arth, 1976; Canil and Fedortchouk, 2001), and the presence of mafic cumulates underneath the exposed alkaline complexes is required by the low whole-rock Ni contents and confirmed by large positive gravity

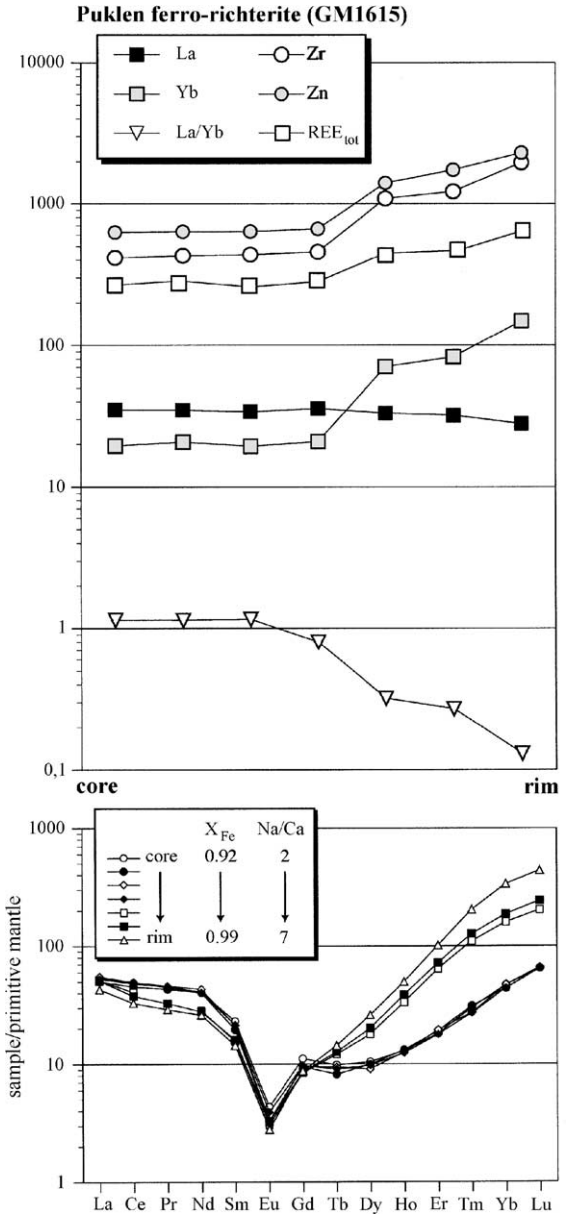

Fig. 9. Zoning profile for selected elements, X_{Fe} and Na/Ca ratio from core to rim of ferro-richterite from Puklen.

and magnetic anomalies centered on the Ilímaussaq area (Blundell, 1978; Forsberg and Rasmussen, 1978). The systematic decrease of Sc concentrations from calcic to sodic clinopyroxenes and amphiboles and within a growing augite (Fig. 4) indicates that fractionation of clinopyroxene was important, as Sc is compatible in clinopyroxene and amphibole within a large range of magma compositions (e.g., Arth, 1976; Mahood and Hildreth, 1983). In Ilímaussaq, amphiboles and clinopyroxenes show an evolution from a pronounced LREE enrichment in the most Ca-rich minerals towards roughly an order of magnitude lower values in the Na-rich compositions, contrary to the trend expected for incompatible trace elements. The same trend can be seen in single minerals, as exemplified in a representative zoning profile of a Na-amphibole from Ilímaussaq (Fig. 11). This feature is best explained by the fractionation of eudialyte, which is a REE-bearing mineral with highly enriched LREE contents compared to HREE (Bailey et al., 2001) and which is ubiquitous in the agpaitic Ilímaussaq rocks.

6.1. Crystal chemical controls on trace element partitioning

Both clinopyroxenes and amphiboles show a continuous development from LREE-enriched patterns in the calcic members via wave-shaped pattern in the sodic–calcic members towards a more pronounced HREE enrichment in the most sodic members (Fig. 10). These principal changes point towards a crystal chemical control on trace element partitioning because of the following arguments:

- The enrichment of HREE in Ca–Na- and especially Na-rich mafic silicates might partly reflect a general preference for trivalent REE as the incorporation of Na^+ requires charge balance with a trivalent ion, following the coupled substitution Na^+ REE⇔2 Ca on the M2 site as proposed for REE partitioning in clinopyroxene (Wood and Blundy, 1997). However, this process should also affect the LREE, which do not show significant enrichment in the Na-rich minerals. Therefore, it seems more likely that there is a particular site preference of the HREE with smaller ionic radii into the optimal sites available in the more Na-rich minerals. HREE were also shown to be compatible in Na-bearing clinopyroxene on the spinel-lherzolite solidus (Blundy et al., 1998).
- For amphiboles, there are multiple crystal-chemical mechanisms for REE^{3+} incorporation and REE are distributed over more than one structural site (Bottazzi et al., 1999) Additionally, it is known that the REE site-preference is mainly a function of

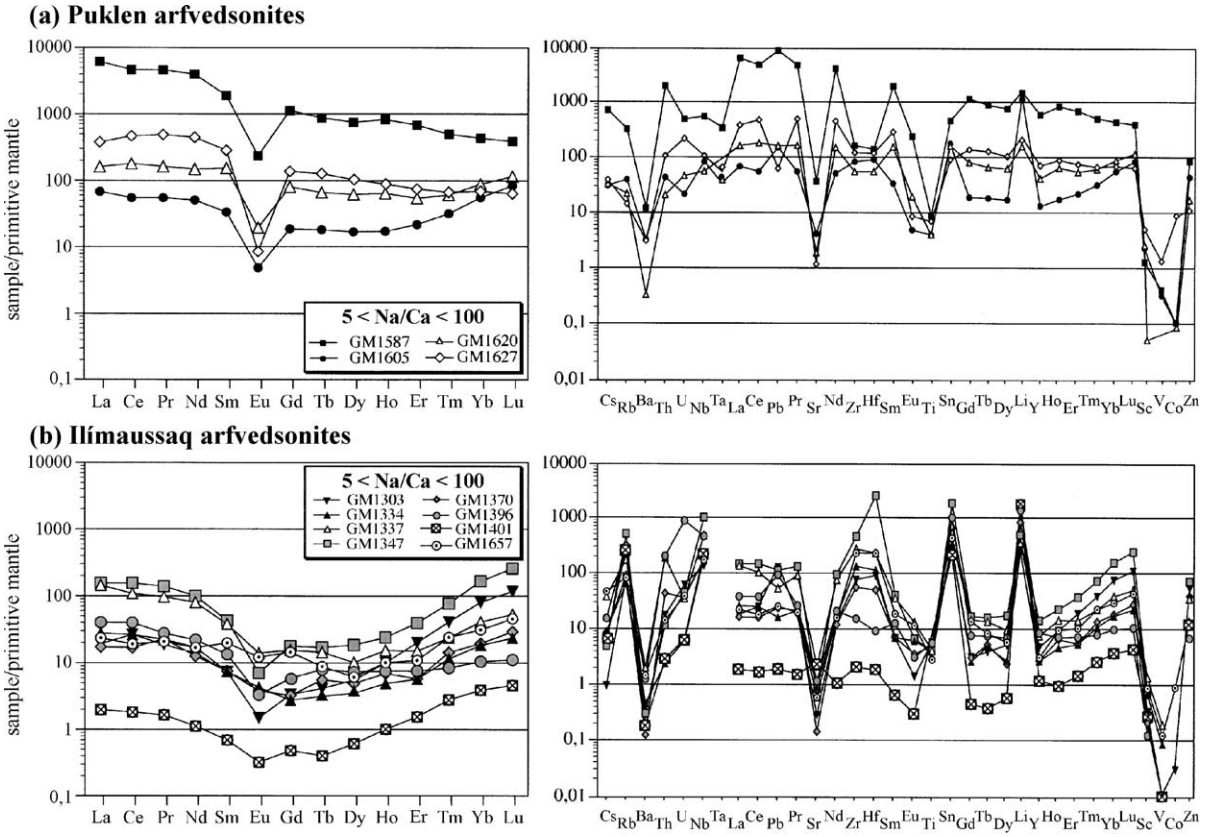

Fig. 10. Averaged mantle-normalized REE and TE patterns for arfvedsonites of (a) Puklen and (b) Ilímaussaq.

major-element composition of the B-group sites in amphiboles (Tiepolo et al., 2000b). This is in agreement with our data, where we observe distinct changes in REE patterns from calcic amphiboles (two Ca^{2+} on B-site) via sodic–calcic amphiboles (B-site occupied by one Ca^{2+} and one Na^{+}) towards sodic amphiboles (two Na^{+} on B-site).

Similarly to the REE, Ti, Zr, Hf and Sn show a systematic behavior in terms of their normalized concentrations in the various pyroxene types. Their normalized concentrations relative to the neighboring elements increase with increasing Na-content in the host mineral. This increase is most pronounced for Zr, Hf and Sn and weaker for Ti. In amphiboles, similar systematics for Zr, Hf and Sn can be observed, whereas Ti remains fairly constant and relatively less depleted throughout the whole amphibole series. The similar geochemical behavior of these elements is probably related to their similar ionic radii and charges (Shannon, 1976). The general increase of Zr, Hf and Sn during fractionation within one single pluton can partly be attributed to enrichment of incompatible elements during closed system fractional crystallization. However, several arguments indicate a major element crystal-chemical control on the contents of these trace elements as well:

- In two of the investigated complexes, significant amounts of Ti-rich magnetite and/or ilmenite crystallized early in their evolution (Larsen, 1976; Marks and Markl, 2001; Marks et al., 2003), probably causing a strong depletion of Ti in the evolving melt. However, in the Ilímaussaq clinopyroxenes, the resulting effect on Ti content in clinopyroxene is surprisingly small: early augites contain only slightly more Ti (up to 5200 ppm) than later aegirines (up to 4200 ppm), and in

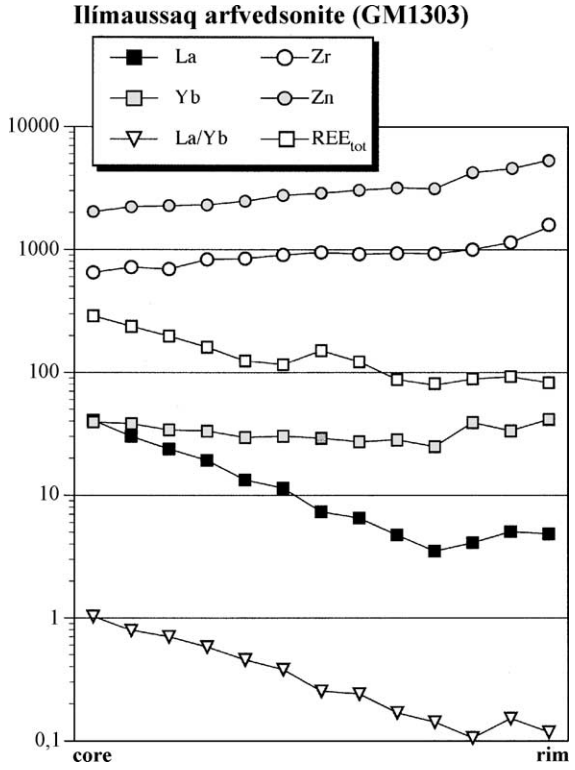

Fig. 11. Zoning profile for selected elements from core to rim of arfvedsonite from Ilímaussaq.

the Puklen rocks early augites are even poorer in Ti (maximum of 5200 ppm) than late-stage aegirines (up to 10,500 ppm).

- Ti-rich aegirines have been described from a number of peralkaline igneous rocks of the Gardar province (Larsen, 1976; Jones and Peckett, 1980; Shearer and Larsen, 1994; Ranlov and Dymek, 1991) and elsewhere (Nielsen, 1979; Piilonen et al., 1998; Njonfang and Nono, 2003). In contrast, Ti-rich augites in more primitive alkali basaltic lavas of the Gardar Province have not been reported so far despite relatively high whole-rock TiO_2 contents of 1.7–3.0 wt.% (Halama et al., 2003) compared to the typically low TiO_2 contents (<0.7 wt.%) in the highly fractionated agpaitic rocks of Ilímaussaq (Bailey et al., 2001).
- For an optimal site of about 0.70 Å in pyroxenes and amphiboles (Jensen, 1973; Bailey et al., 2001), Zr^{4+} (0.72 Å), Hf^{4+} (0.71 Å) and Sn^{4+} (0.69 Å) fit fairly well, whereas Ti^{4+} (0.61 Å) is considerably smaller (Shannon, 1976). This relatively large mismatch of Ti might contribute to the rather weak increase in Ti contents during fractionation compared to Zr, Hf and Sn.
- Positive Zr–Hf anomalies are only present in Ca–Na- and Na-dominated clinopyroxenes and amphiboles, but not in the calcic varieties, again suggesting a crystal-chemical control. An enrichment of Zr and Hf due to prolonged fractional crystallization alone is not a viable explanation since the neighboring elements do not show such an extreme enrichment.
- In the Ilímaussaq intrusion, late-stage hydrothermal mineralizations containing rare Sn silicates like Sørensenite ($Na_4SnBe_2(OH)_4Si_6O_{16}$) are well known (Semenov et al., 1965). Thus, one can argue that the high Sn contents in late aegirines compared to earlier augites are an effect of fractionation and enrichment of Sn. However, the relatively high Sn contents and strikingly positive Sn anomalies in the Grønnedal-Ika aegirine–augites argue against this, since these pyroxenes are invariably early magmatic phases.

Among the transition metals, Zn^{2+} has an ionic radius of 0.74 Å in sixfold coordination, which is very similar to the ionic radius of Sc^{3+} (0.745 Å) (Shannon, 1976). Since the compatibility of Sc in clinopyroxene and amphibole is well known, it is likely that the Zn^{2+} ion with a similar ionic radius may have a similar degree of compatibility, which can explain the enrichment in normalized Zn contents in both clinopyroxene and amphibole compared to primitive mantle.

6.2. Lithium: influence of the melt composition

In the clinopyroxenes, Li behaves quite variable with flat patterns or small positive peaks in the mantle-normalized augite patterns, negative peaks in the aegirine–augites and positive peaks in the aegirines. The enrichment level is also quite different, depending on the complex: clinopyroxenes from Ilímaussaq have medium values of ~20–40×, from Puklen ~100× and from Grønnedal-Ika <7× primitive mantle values, apparently independent of the mineral composition. This indicates that Li contents in the clinopyroxenes are mainly dependent on the melt composition. The Puklen melts were relatively most enriched in Li, whereas the Grønnedal-Ika melts had

relatively low Li contents. The generally positive Li peaks in amphiboles, however, particularly in the sodic members, are clearly an effect of preferential partitioning of Li into amphibole, and it was shown by Hawthorne et al. (1993, 1994) that Li could be a major component in Na-amphiboles from peralkaline igneous rocks.

6.3. Crustal contamination

Based on Nd isotopic data, crustal contamination plays a major role in the Puklen rocks (Marks et al., 2003). In the following, we will use these data as indicators for crustal contamination and discuss the influence on the incorporation of some elements into clinopyroxene and amphibole.

Syenites show a range of ε_{Nd} values between −3.8 and −7.2, and alkali granites vary between −5.9 and −9.6. Within the syenites, samples GM1593 (ε_{Nd}=−7.2) and GM1600 (ε_{Nd}=−6.4) are the most contaminated ones. Augites of these two samples have the highest contents in U, Pb, V and Zn, but the lowest concentrations of Ti, Zr and Hf. This is consistent with assimilation of crustal rocks, which have high contents of U, Pb, V and Zn, and low contents of Ti, Zr and Hf compared to the primitive mantle (Rudnick and Fountain, 1995; McDonough and Sun, 1995). These two samples are also those with positive Pb anomalies (Fig. 3). We defined a Pb/Pb* value, which was calculated similar to Eu/Eu*, as the geometric mean $Pb/Pb^* = Pb_N\sqrt{(Ce_N \cdot Pr_N)}$. This should be a useful parameter, since Ce and Pr normally have similar normalized values. The significant correlation between Pb/Pb* and ε_{Nd} values in Fig. 12 confirms the influence of crustal contamination on this parameter and provides evidence of a relation between trace element composition in minerals and assimilation processes during the magmatic evolution of an alkaline complex. The same argument may also hold for the differences in primary Li melt contents discussed above.

6.4. Partitioning of trace elements between coexisting clinopyroxene and amphibole

To establish meaningful intermineral partition coefficients, chemical equilibrium is required, which is, however, often difficult to evaluate (e.g., Chazot et al., 1996). We calculated clinopyroxene–amphibole trace element abundance ratios for selected samples where textural and isotopic criteria (Markl et al., 2001b; Marks et al., 2003) indicate equilibrium conditions (Fig. 13a–d; Table 5). These values might not strictly be interpreted as partition coefficients but can act as useful guides for trace element partitioning in alkaline magmatic rocks in general and will be used here as an approximation for equilibrium partition coefficients.

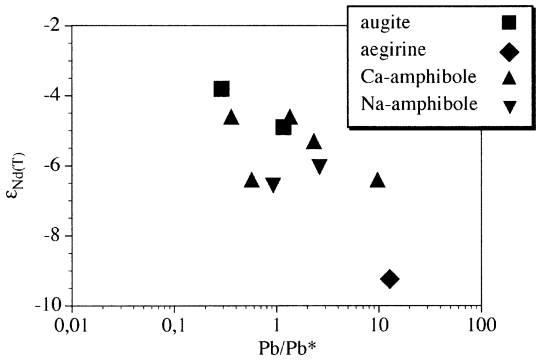

Fig. 12. ε_{Nd} vs. Pb/Pb* diagram for mineral separates of the Puklen rocks. ε_{Nd} data from Marks et al. (2003). See text for definition of Pb/Pb*.

Calculated clinopyroxene–amphibole partition coefficients ($D_{cpx-amph}$) for the majority of trace elements vary for the Ilímaussaq augite syenites (Fig. 13a) between 0.1 and 0.6. In the Puklen syenites (Fig. 13b), they are slightly higher (between 0.6 and 1.7). In the Na–Ca system of Grønnedal-Ika (Fig. 13c), a larger range between 0.3 and 2.7 is observed. Finally, in the Na-dominated system of Ilímaussaq (Fig. 13d) they vary between 0.07 and 0.9. For a specific element, the determined $D_{cpx-amph}$ values for the whole sample suite vary within about 1 order of magnitude. However, samples with similar major element chemical composition show similar patterns, despite certain differences in the absolute D values. This points to the reasonable assumption of chemical equilibrium between the respective mineral pairs. Thus, clinopyroxene–amphibole partition coefficients seem to be relatively independent of major element mineral compositions, and no systematic variation of D values with increasing Na-content of clinopyroxene and amphibole can be observed. This provides an interesting tool to assess the equilibration of clinopyroxene, amphibole and melt in magmatic systems.

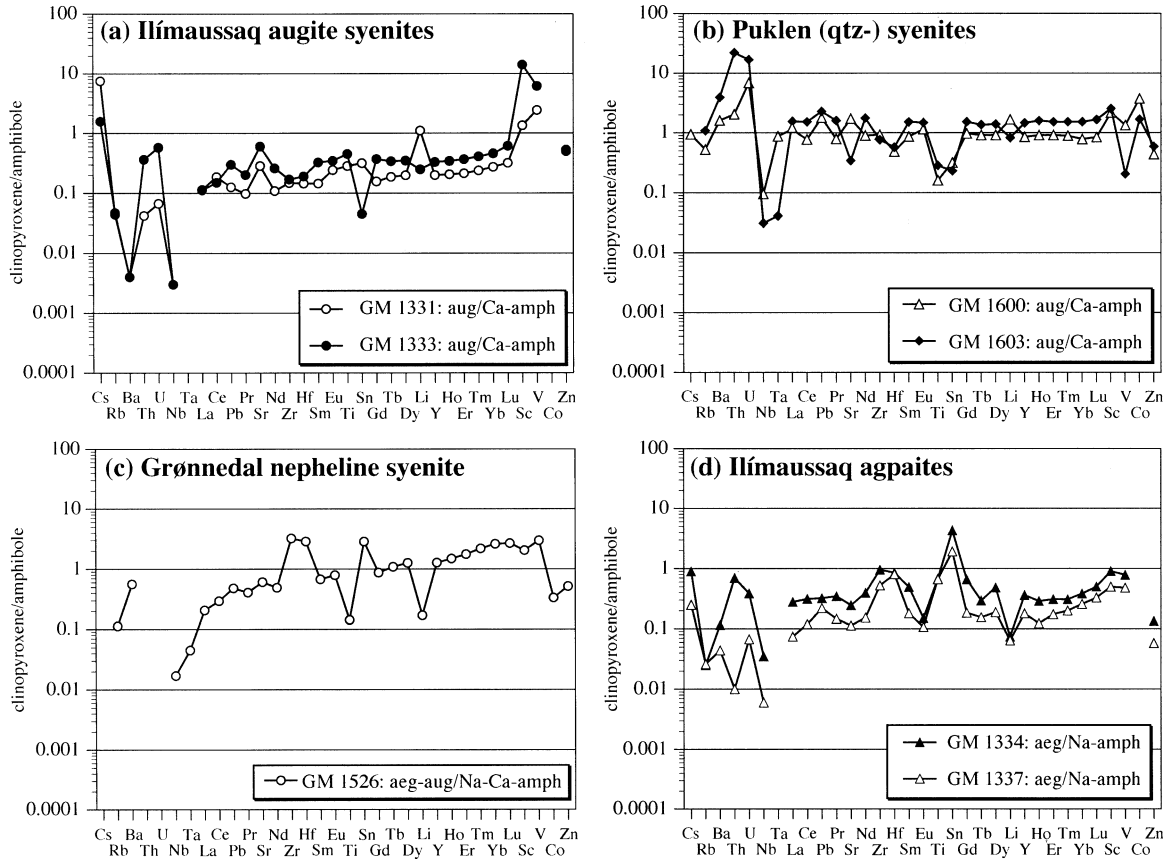

Fig. 13. Clinopyroxene/amphibole partition coefficients for (a) Ilímaussaq augite syenites, (b) Puklen syenites, (c) Grønnedal nepheline syenite and (d) Ilímaussaq agpaites.

Overall, our calculated $D_{cpx-amph}$ values span a comparable range as literature data for ultramafic (Vannucci et al., 1991; Chazot et al., 1996; Grègoire et al., 2000), basanitic (Irving and Frey, 1984; Adam and Green, 1994) and more evolved compositions (Villemant et al., 1981; Wörner et al., 1983; Lemarchand et al., 1987) do ($D_{cpx-amph}$ ~0.1 to ~10). There are no systematic changes in absolute $D_{cpx-amph}$ values with SiO_2 content or alkalinity, which indicates that trace element partitioning between clinopyroxene and amphibole is not significantly influenced by the melt composition. This is interpreted to be due to the principally similar crystal structures and cation sites of these two minerals. Some elements exhibit noteworthy features:

- Nb and Ta always have a strong preference for amphibole, which is in accordance with previous studies on mantle minerals (e.g., Witt-Eickschen and Harte, 1994; Chazot et al., 1996) and andesitic melts (Brenan et al., 1995). U and Th are also preferentially incorporated into amphibole except for the Puklen samples.
- Rb and Ba are apparently less compatible in clinopyroxene than in amphibole, which is consistent with previous studies (e.g., Brenan et al., 1995; Chazot et al., 1996). This is caused by a strong preference of these two elements for the A-site in amphibole (e.g., Dalpè and Baker, 2000), which has no equivalent position in pyroxene. As for U and Th, Rb and Ba in the Puklen syenites have significantly higher $D_{cpx-amph}$ values. This might be caused by secondary fluid circulation, which was shown to disturb the Rb/Sr isotopic system in the Puklen minerals (Marks et al., 2003).

Table 5
Clinopyroxene–amphibole distribution coefficients for alkaline igneous rocks

Complex	Ilímaussaq	Ilímaussaq	Ilímaussaq	Ilímaussaq	Puklen	Puklen	Gronnedal-Ika
Rock type	Augite syenite	Augite syenite	Agpaite	Agpaite	Quartz syenite	Quartz syenite	Nepheline syenite
Mineral pair	Augite–ferro-pargasite	Augite–ferro-pargasite	Aegirine–arfvedsonite	Aegirine–arfvedsonite	Augite–ferro-edenite	Augite–ferro-edenite	Aegirine–augite-katophorite
Sample	GM 1331	GM 1333	GM 1334	GM 1337	GM 1600	GM 1603	GM 1526
Cs	7.50	1.57	0.90	0.25	0.94		
Rb	0.04	0.05	0.03	0.03	0.52	1.08	0.11
Ba	0.004	0.004	0.12	0.04	1.60	3.92	0.56
Th	0.04	0.36	0.70	0.01	2.04	22.10	
U	0.07	0.58	0.38	0.07	6.84	16.92	
Nb	0.003	0.003	0.04	0.01	0.10	0.03	0.02
Ta					0.87	0.04	0.04
La	0.11	0.11	0.28	0.07	1.23	1.55	0.21
Ce	0.19	0.15	0.31	0.12	0.77	1.52	0.29
Pb	0.13	0.30	0.32	0.22	1.78	2.28	0.48
Pr	0.10	0.20	0.35	0.15	0.79	1.59	0.41
Sr	0.29	0.60	0.24	0.11	1.72	0.34	0.61
Nd	0.11	0.26	0.39	0.15	0.90	1.76	0.49
Zr	0.15	0.17	0.96	0.52	0.93	0.76	3.24
Hf	0.15	0.19	0.85	0.80	0.49	0.57	2.88
Sm	0.15	0.33	0.49	0.18	0.86	1.52	0.67
Eu	0.24	0.35	0.15	0.11	1.15	1.48	0.79
Ti	0.28	0.45	0.68	0.66	0.16	0.28	0.14
Sn	0.32	0.05	4.32	1.92	0.32	0.23	2.87
Gd	0.16	0.37	0.66	0.18	0.97	1.52	0.87
Tb	0.19	0.34	0.29	0.15	0.91	1.36	1.09
Dy	0.20	0.35	0.48	0.19	0.91	1.39	1.26
Li	1.10	0.25	0.07	0.06	1.66	0.82	0.17
Y	0.20	0.33	0.36	0.18	0.85	1.46	1.28
Ho	0.21	0.35	0.29	0.12	0.91	1.59	1.49
Er	0.21	0.37	0.31	0.17	0.91	1.52	1.76
Tm	0.24	0.41	0.31	0.20	0.89	1.52	2.19
Yb	0.27	0.46	0.38	0.26	0.78	1.52	2.62
Lu	0.32	0.61	0.50	0.33	0.84	1.66	2.69
Sc	1.35	14.13	0.90	0.50	2.17	2.53	2.05
V	2.43	6.17	0.78	0.48	1.33	0.20	2.99
Co					3.72	1.67	0.33
Zn	0.53	0.50	0.14	0.06	0.44	0.59	0.52

- $D_{cpx–amph}$ values for Sr are characterized by small positive peaks in the Ca-rich system, but slight depressions in the Na-rich system. The two Puklen samples behave variable, which may be an effect of secondary metasomatism, as mentioned above (Marks et al., 2003).
- Zr, Hf and Sn develop a preference for clinopyroxene as the system evolves towards Ca–Na and Na-rich compositions, but absolute D_{Zr} and D_{Hf} values >1 only occur in the Ca–Na system (Grønnedal-Ika). For Zr and Hf, literature data are contradictory, indicating similar compatibilities in andesitic rocks (Brenan et al., 1995), variable behavior (Vannucci et al., 1991) or a preference for amphibole (Chazot et al., 1996) in ultramafic rocks.
- The $D_{cpx–amph}$ values of the REE are continuously increasing from the LREE towards the HREE in the Ilímaussaq and Grønnedal-Ika rocks. However, whereas in Ilímaussaq, all D_{REE} are <1, D_{REE} values in Grønnedal-Ika increase from D_{La}=0.2 towards D_{Lu}=2.7, i.e., the LREE partition preferentially into amphibole, but the HREE do not. In contrast, DREE values for Puklen syenites are

fairly constant. For the REE, Klein et al. (1997) assumed that as a consequence of nearly identical values of Young's moduli and lattice site geometries of M4- and M2-sites in amphibole and clinopyroxene, respectively, $D_{cpx-amph}$ should be identical for all REE, and, consequently, REE patterns of clinopyroxenes and amphiboles should be subparallel. Measured REE partition coefficients between clinopyroxene and amphibole in mantle rocks (Witt-Eickschen and Harte, 1994; Chazot et al., 1996) partly confirm this assumption as our data for the Puklen syenites do (Figs. 3a, 7a and 13b). However, Witt-Eickschen and Harte (1994) also found a slight tendency of increase of $D_{cpx-amph}$ for the REE with increasing Na-content, which is not confirmed by our data. The tendency of increase of $D_{cpx-amph}$ values from La to Lu found by Witt-Eickschen and Harte (1994) in mantle rocks and by Irving and Frey (1984) for basanitic rocks is in accordance with our results for the Ilímaussaq and Grønnedal-Ika rocks, but not for the Puklen syenites.

6.5. Evaluation of mineral–melt partition coefficients for alkaline systems

Published partition coefficients for alkaline systems (Larsen, 1979; Wörner et al., 1983; Lemarchand et al., 1987) show a scatter, which is surprisingly large even when differences in the mineral compositions are taken into account. Thus, we calculated coexisting melt compositions using minimum and maximum mineral–melt partition coefficients reported (Table 6; Figs. 14 and 15). To evaluate the accuracy of the partition coefficients, knowledge of the trace element composition of the melt is required. Since whole-rock compositions of the intrusive rocks of the investigated complexes are unlikely to represent melts due to accumulation processes (particularly of feldspar), we used compositions of fine-grained dike rocks that are considered as possible initial melt compositions for the Ilímaussaq plutonic rocks (Table 6). The possible initial melt of the augite syenite might be resembled by an aphyric marginal facies sample from an alkali olivine basalt of the older giant dike complex (OGDC) of

Table 6
Maximum and minimum partition coefficients for alkaline rocks used to calculate melt compositions and "initial magma" compositions

Element	$D_{clinopyroxene-melt}$		$D_{amphibole-melt}$		"Initial magmas"	
	D_{max}	D_{min}	D_{max}	D_{min}	OGDC (in ppm)	Ilímaussaq (in ppm)
Cs	0.05	0.03				6.99
Rb	0.04	0.02	0.14	0.11	27	360
Ba	0.02	0.01	5.58	0.39	1477	36
Th	0.15	0.01	0.07	0.03		63
U	0.09	0.02	0.45	0.06		29
Nb	0.03	0.03			25	867
Ta	0.50	0.21	1.25	0.85		
La	0.66	0.06	0.99	0.22	39.3	483
Ce	0.96	0.21	2.06	1.05	89.3	845
Pb	0.13	0.10				71
Sr	0.25	0.25	9.77	3.00	1186	50
Nd	2.27	0.49	3.56	2.53	51.9	298
Zr	1.02	0.24	1.77	0.37	136	4231
Hf	1.54	0.40	1.19	0.54		90
Sm	6.18	0.48	7.29	2.12	9.4	39.3
Eu	13.87	0.60	9.39	1.07	3.5	3.40
Tb	8.63	0.60	9.74	1.45		7.64
Tm	0.79	0.35	2.00	0.92		
Yb	2.63	0.40	2.10	0.33	2.2	34.2
Lu	2.06	0.41	2.83	1.08	0.3	
Sc	334	4.05	120.7	0.90	14	

Partition coefficients from Larsen (1979), Wörner et al. (1983) and Lemarchand et al. (1987). "Initial magmas" are a chilled marginal facies sample from an alkali olivine basalt of the OGDC (Upton et al., 1985) and an eudialyte-bearing nepheline–porphyritic phonolitic dike associated with the Ilímaussaq complex (Larsen and Steenfelt, 1974; Larsen, 1979).

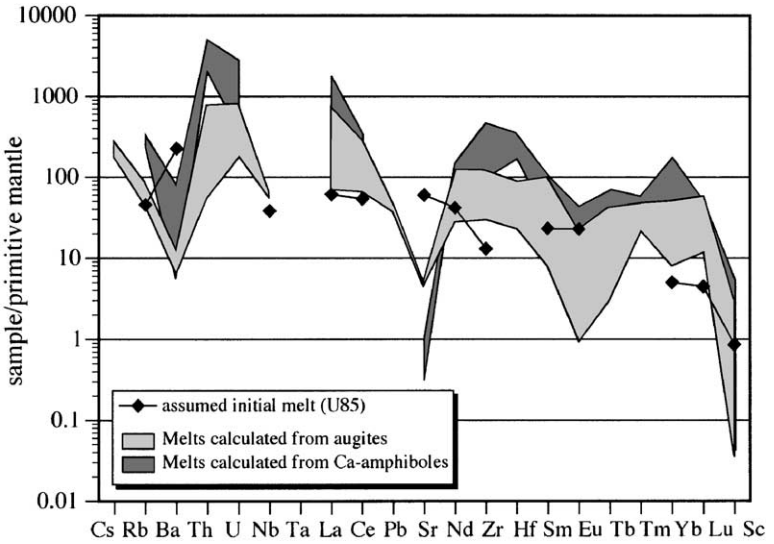

Fig. 14. Comparison of calculated melts, using the partition coefficient listed in Table 6, with the assumed initial melt, which is an aphyric marginal facies sample from an alkali olivine basalt of the older giant dike complex (OGDC) of Tugtutùq (Upton et al., 1985).

Tugtutôq (Upton et al., 1985). This dike rock is similar in age and close to the Ilímaussaq complex. It is a fine-grained, well-chilled rock, with high Sr contents (Table 6) and no Eu-anomaly, indicating that this rock had undergone no significant plagioclase fractionation at the time of emplacement. A very fine grained peralkaline dike rock described by Larsen and Steenfelt (1974) and by Larsen (1979) is used as approximation for the initial peralkaline Ilímaussaq magma. Detailed mineral, chemical, petrological and isotopic investigations of Marks and Markl (2003) on this dike rock confirm the early assumption of Larsen and Steenfelt (1974) that this dike rock is closely related to the initial peralkaline Ilímaussaq magma. For example, the different mineral assemblages found in this dike rock can be correlated to the various types of plutonic rocks of the Ilímaussaq complex. The intrusive complexes of Puklen and Grønnedal-Ika are not investigated further here since for these complexes no such dike rocks which could represent melt compositions exist.

By comparing the assumed initial melt composition with the calculated melts from augites, we note that Ba, Sr and Eu in the Ilímaussaq calculated melts tend to show marked negative spikes and lower concentrations than the assumed initial melt, which is most probably the effect of accumulation of feldspar. However, for other elements (except U and Zr) melt compositions calculated from augites show a good agreement with the assumed initial melt for the augite syenite (Fig. 14). If melt compositions are calculated from Ca-amphiboles, positive deviations in the melt compared to the whole-rock values occur for Th, U, La, Ce, Nd, Zr, Hf, Yb and Lu (Fig. 14). This is possibly related to their late-magmatic formation under more hydrous conditions.

A crystal-chemical control on REE partitioning between clinopyroxene and melt is suggested when the clinopyroxene compositions with low Na contents used in the previous studies (Larsen, 1979; Wörner et al., 1983; Lemarchand et al., 1987) and the theoretical model of Wood and Blundy (1997) (WB97 model) are considered in comparison to the Na-rich aegirine (Fig. 15). To evaluate this more quantitatively, we calculated partition coefficients for the REE (D_{REE}) from known clinopyroxene compositions after the model of Wood and Blundy (1997) (WB97 model). Examples of the calculated D_{REE} values are listed in Table 7 and the results are shown graphically in Fig. 15a. These calculations show that the apex of the parabolic curve trends towards smaller ionic radii as the clinopyroxene becomes more Na–Fe^{3+}-rich. This means that the HREE become more compatible relative to the LREE, which is in qualitative agreement with the observed increase in HREE concentrations in aegirine–augites and aegirines (Figs. 5 and 6). Calculated D_{REE} for augite and Mg-rich aegirine–

augite cores where Fe^{2+} dominates over Fe^{3+} (Table 7) agree fairly well with data from natural samples (Table 6), but for aegirine–augite rims and aegirines they tend to be lower.

In Fig. 15b and c, melt compositions calculated using the DREE determined from the Wood and Blundy (1997) model and using the D_{REE} derived from natural samples are compared to whole-rock data and possible melt compositions from Ilímaussaq. For the augite syenite (Fig. 15b), the melts calculated after the WB97 model show a good overlap with the assumed initial melt, as well as with whole-rock data for the Ilímaussaq augite syenite (Bailey et al., 2001), except for Eu. This confirms the applicability of the theoretical model to augitic clinopyroxenes in alkaline systems. In contrast, melts calculated from a typical aegirine using either D_{REE} derived from natural samples or after the WB97 model (Fig. 15c) have lower REE contents than the assumed initial peralkaline melt (Larsen and Steenfelt, 1974; Larsen, 1979; see above) and agpaitic whole-rocks (Bailey et al., 2001), and the most significant deviations occur when the lowest aegirine formation temperatures are assumed. However, there is a reasonable overlap between the WB97 model melts and melts calculated with the D_{REE} from natural samples, but the WB97 model melts tend to higher LREE and lower HREE concentrations. Despite the consideration of crystal-chemical effects, the partition coefficients calculated after the WB97 model appear not to be suitable to calculate melt compositions from aegirines. This theoretical model was based on clinopyroxenes with high Mg numbers, which does not apply to the formation of Mg-poor aegirine. Furthermore, Wood and Blundy (1997) also note that compositions containing substantial amounts of the $NaFe^{3+}Si_2O_6$ component deviate from the simple activity–composition relationship used in their model.

In summary, partition coefficients derived from natural samples and derived from the theoretical model of Wood and Blundy (1997) can be used for calculating melt compositions from clinopyroxenes

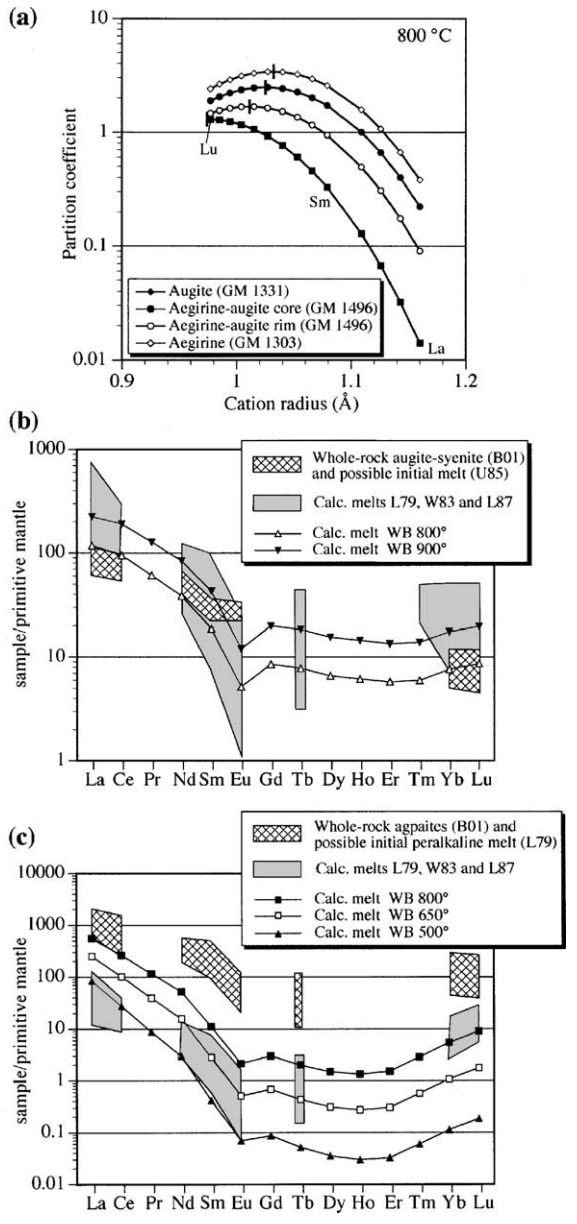

Fig. 15. (a) Clinopyroxene–melt REE partition coefficients calculated form mineral chemical data at P=1 kbar for different representative clinopyroxene compositions at 800 °C after Wood and Blundy (1997). Dark grey vertical bars mark the position of r_0 (see Table 7 for data and explanations). (b) Primitive mantle-normalized REE plots of calculated melts and comparative whole-rock data for the Ilímaussaq augite syenite (c) for the Ilímaussaq agpaitic rocks. L79, W83 and L87 denote melts calculated with a range of partition coefficients from Larsen (1979), Wörner et al. (1983) and Lemarchand et al. (1987) listed in Table 6. WB denotes melts calculated with the partition coefficients derived from the theoretical model of Wood and Blundy (1997) listed in Table 7. Whole-rock data are from Bailey et al. (2001) (B01), Upton et al. (1985) (U85) and Larsen (1979) (L79).

Table 7
Selected typical mineral compositions and REE partition coefficients calculated from the crystal chemistry after the theoretical model of Wood and Blundy (1997) for 800 °C and 0.1 GPa

Mineral	Augit	Aegirine–augite, core	Aegirine–augite, rim	Aegirine
Intrusion	Ilímaussaq	Grønnedal	Grønnedal	Ilímaussaq
Sample	GM 1331	GM 1496	GM 1496	GM 1303
Cations (pfu)				
Si	1.924	1.943	1.984	2.002
$Al^{(IV)}$	0.076	0.057	0.016	0.000
$Al^{(VI)}$	0.002	0.057	0.033	0.006
Ti	0.026	0.010	0.009	0.016
Fe^{3+}	0.062	0.145	0.395	0.942
Mg	0.601	0.389	0.225	0.004
Fe^{2+}	0.391	0.416	0.302	0.041
Mn	0.016	0.012	0.022	0.003
Ca	0.862	0.804	0.584	0.003
Na	0.039	0.166	0.428	0.983
Total	4.000	4.000	4.000	4.000
Calculated parameters				
r_0	1.032	1.025	1.011	0.974
E_{M2} at P, T	280.7	280.7	280.7	280.7
Mg# melt	0.22	0.11	0.05	0.0004
D_0^{3+}	3.41	2.48	1.68	1.30
Calculated partition coefficients after Wood and Blundy (1997)				
D_{La}	0.38	0.22	0.09	0.01
D_{Ce}	0.66	0.40	0.17	0.03
D_{Pr}	1.07	0.66	0.31	0.07
D_{Nd}	1.57	1.00	0.49	0.13
D_{Sm}	2.57	1.72	0.94	0.33
D_{Eu}	2.94	2.01	1.16	0.45
D_{Gd}	3.22	2.25	1.35	0.60
D_{Tb}	3.38	2.42	1.52	0.76
D_{Dy}	3.41	2.48	1.63	0.92
D_{Ho}	3.30	2.45	1.68	1.06
D_{Er}	3.12	2.35	1.67	1.16
D_{Tm}	2.88	2.21	1.62	1.24
D_{Yb}	2.64	2.05	1.55	1.28
D_{Lu}	2.40	1.89	1.46	1.30
DLa/D_{Lu}	0.112	0.089	0.055	0.015

r_0 is the radius of the ion that would ideally fit into the crystallographic site of interest, E_{M2} is the Young's modulus of the M2-site in clinopyroxene and D_0^{3+} is the partition coefficient of the element with the radius r_0. Mg# melt was estimated from the pyroxene composition after Wood and Blundy (1997).

with low Na–Fe^{3+}-contents, but they do not yield reliable melt compositions when Na–Fe^{3+}-rich clinopyroxene or amphibole data are taken. Therefore, experimental data on trace element partitioning in alkaline Fe^{3+}-rich systems would be highly desirable to improve the theoretical model and obtain more accurate partition coefficients for those systems.

7. Summary and concluding remarks

This comparative study on trace element contents in mafic minerals of three alkaline igneous complexes confirms that trace element contents of amphiboles and clinopyroxenes are mainly influenced by two factors: whereas the major element composition of the host mineral exerts the dominant control on the partitioning behavior of the trace elements (e.g., Blundy and Wood, 2003), changes in the melt composition during magmatic processes such as fractionation, crustal assimilation and fluid interaction naturally influence the absolute and/or relative concentrations. We show that clinopyroxenes and amphiboles show a continuous development from LREE-enriched patterns in the calcic minerals via wave-shaped pattern in the Ca–Na minerals towards a more pronounced HREE enrichment in the most Na-rich minerals and an increase in Zr, Hf, Sn and HREE concentrations with increasing Na/Ca ratio. These features appear to be related to an increasing preference of these elements for the mineral structure as the magmatic evolution proceeds. Calculations of clinopyroxene–melt partition coefficients based on a theoretical model after Wood and Blundy (1997) show that HREE relative to LREE are more easily incorporated into the crystal structure as the system becomes more Na–Fe^{3+}-rich, which is in qualitative agreement with the observed REE concentrations.

The partitioning of most trace elements between clinopyroxene and amphibole seems to be fairly independent of melt composition or major element composition of the host crystals. Most trace elements show a slight preference for amphibole, which is most pronounced for Nb, Ta, U, Th, Rb, Ba and Li. In contrast, Zr, Hf and Sn develop a preference for clinopyroxene relative to the neighboring elements, as the system evolves from a Ca-dominated to a Na-dominated one.

For evolved alkaline to peralkaline magmatic systems, published clinopyroxene–melt partition coefficients from the literature may be used with some confidence only if the clinopyroxene has a similar crystal composition, i.e., if it is broadly diopsidic to augitic. Partition coefficients based on the theoretical model of Wood and Blundy (1997) are also applicable for clinopyroxenes in alkaline systems, but only if the

mineral is relatively poor in Fe^{3+}. For clinopyroxenes containing considerable amounts of $NaFe^{3+}Si_2O_6$, neither the published partition coefficients nor the partition calculated on the basis of the crystal chemistry (Wood and Blundy, 1997) appears to be adequate.

Acknowledgements

Laser ICP-MS measurements were carried out at the Large Scale Geochemical Facility supported by the European Community—Access to Research Infrastructure action of the Improving Human Potential Programme, contract number HPRI-CT-1999-00008 awarded to Prof. B. J. Wood (University of Bristol) which is gratefully acknowledged. Bruce Paterson provided invaluable help during these measurements. Financial support for this work was granted by the Deutsche Forschungsgemeinschaft (grant Ma-2135/1-2). Constructive reviews of James Brenan and John Adam and the editorial work of Roberta Rudnick and Tim Horscroft are greatly appreciated. **[RR]**

References

Adam, J., Green, T.H., 1994. The effects of pressure and temperature on the partitioning of Ti, Sr and REE between amphibole, clinopyroxene and basanitic melts. Chem. Geol. 117, 219–233.

Adam, J., Green, T., 2003. The influence of pressure, mineral composition and water on trace element partitioning between clinopyroxene, amphibole and basanitic melts. Eur. J. Mineral. 15, 831–841.

Allaart, J.H., 1976. Ketilidian mobile belt in South Greenland. In: Escher, A., Watt, W.S. (Eds.), Geology of Greenland. Grønlands Geologiske Undersøgelse, pp. 121–151.

Armstrong, J.T., 1991. Quantitative elemental analysis of individual microparticles with electron beam instruments. In: Heinrich, K.F.J., Newbury, D.E. (Eds.), Electron Probe Quantitation. Plenum, New York, pp. 261–315.

Arth, J.G., 1976. Behaviour of trace elements during magmatic processes-a summary of theoretical models and their applications. J. Res. U.S. Geol. Surv. 4, 41–47.

Bailey, J.C., Gwozdz, R., Rose-Hansen, J., Sørensen, H., 2001. Geochemical overview of the Ilimaussaq alkaline complex, South Greenland. Geol. Greenl. Surv. Bull. 190, 35–53.

Bedford, C.M., 1989. The mineralogy, geochemistry and petrogenesis of the Grønnedal-Ika complex, southwest Greenland. Unpublished PhD thesis, University of Durham.

Bennett, S.L., Blundy, J., Elliott, T., 2003. The effect of sodium and titanium on crystal-melt partitioning of trace elements. Geochim. Cosmochim. Acta 68, 2335–2347.

Benoit, M., Polvè, M., Ceuleneer, G., 1996. Trace element and isotopic characterization of mafic cumulates in a fossil mantle diapir (Oman ophiolite). Chem. Geol. 134, 199–214.

Blundell, D.J., 1978. A gravity survey across the Gardar Igneous Province, SW Greenland. J. Geol. Soc. (Lond.) 135, 545–554.

Blundy, J., Dalton, J., 2000. Experimental comparison of trace element partitioning between clinopyroxene and melt in carbonate and silicate systems, and implications for mantle metasomatism. Contrib. Mineral. Petrol. 139, 356–371.

Blundy, J.D., Wood, B.J., 1991. Crystal-chemical controls on the partitioning of Sr and Ba between plagioclase feldspar, silicate melts, and hydrothermal solutions. Geochim. Cosmochim. Acta 55, 193–209.

Blundy, J., Wood, B., 1994. Prediction of crystal-melt partition coefficients from elastic moduli. Nature 372, 452–454.

Blundy, J., Wood, B., 2003. Partitioning of trace elements between crystals and melts. Earth Planet. Sci. Lett. 210, 383–397.

Blundy, J.D., Robinson, J.A.C., Wood, B.J., 1998. Heavy REE are compatible in clinopyroxene on the spinel lherzolite solidus. Earth Planet. Sci. Lett. 160, 493–504.

Bottazzi, P., Tiepolo, M., Vannucci, R., Zanetti, A., Brum, R., Foley, S.F., Oberti, R., 1999. Distinct site preferences for heavy and light REE in amphibole and the prediction of $^{Amph/L}D_{REE}$. Contrib. Mineral. Petrol. 137, 36–45.

Brenan, J.M., Shaw, H.F., Ryerson, F.J., Phinney, D.L., 1995. Experimental determination of trace-element partitioning between pargasite and a synthetic hydrous andesitic melt. Earth Planet. Sci. Lett. 135, 1–11.

Bridgwater, D., 1967. Feldspathic inclusions in the Gardar igneous rocks of South Greenland and their relevance to the formation of major anorthosites in the Canadian Shield. Can. J. Earth Sci. 4, 995–1014.

Bridgwater, D., Harry, W.T., 1968. Anorthosite xenoliths and plagioclase megacrysts in Precambrian intrusions of South Greenland. Medd. Grønl. 185 (243 pp.).

Canil, D., Fedortchouk, Y., 2001. Olivine-liquid partitioning of vanadium and other trace elements, with applications to modern and ancient picrites. Can. Mineral. 39, 319–330.

Chazot, G., Menzies, M., Harte, B., 1996. Determination of partition coefficients between apatite, clinopyroxene, amphibole, and melt in natural spinel lherzolites from Yemen: implications for wet melting of the lithospheric mantle. Geochim. Cosmochim. Acta 60, 423–437.

Coogan, L.A., Kempton, P.D., Saunders, A.D., Norry, M.J., 2000. Melt aggregation within the crust beneath the Mid-Atlantic Ridge: evidence from plagioclase and clinopyroxene major and trace element compositions. Earth Planet. Sci. Lett. 176, 245–257.

Costa, F., Chakraborty, S., Dohmen, R., 2003. Diffusion coupling between trace and major elements and a model for calculation of magma residence times using plagioclase. Geochim. Cosmochim. Acta 67, 2189–2200.

Dalpè, C., Baker, D.R., 2000. Experimental investigation of large-ion-lithophile-element-, high-field-strength-element- and rare-

earth-element-partitioning between calcic amphibole and basaltic melt: the effects of pressure and oxygen fugacity. Contrib. Mineral. Petrol. 140, 223–250.

Drake, M.J., Weill, D.F., 1975. Partitioning of Sr, Ba, Ca, Y, Eu^{2+}, Eu^{3+} and other REE between plagioclase feldspar and magmatic liquid: an experimental study. Geochim. Cosmochim. Acta 39, 689–712.

Emeleus, C.H., 1964. The Grønnedal-Ika alkaline complex, South Greenland. The structure and geological history of the complex. Medd. Grønl. 172 (75 pp.).

Escher, A., Watt, W.S., 1976. Geology of Greenland. Geological Survey of Greenland, Copenhagen. 603 pp.

Ferguson, J., 1964. Geology of the Ilimaussaq alkaline intrusion, South Greenland. Bull.-Grønl. Geol. Unders. 39 (82 pp.).

Forsberg, R., Rasmussen, K.L., 1978. Gravity and rock densities in the Ilimaussaq area, South Greenland. Rapp.-Grønl. Geol. Unders. 90, 81–84.

Garde, A.A., Hamilton, M.A., Chadwick, B., Grocott, J., McCaffrey, K.J.W., 2002. The Ketilidian orogen of South Greenland: geochronology, tectonics, magmatism, and fore-arc accretion during Palaeoproterozoic oblique convergence. Can. J. Earth Sci. 39, 765–793.

Grègoire, M., Moine, B.N., O'Reilly, S.Y., Cottin, J.Y., Giret, A., 2000. Trace element residence and partitioning in mantle xenoliths metasomatized by highly alkaline, silicate- and carbonate-rich melts (Kerguelen Islands, Indian Ocean). J. Petrol. 41, 477–509.

Halama, R., Waight, T., Markl, G., 2002. Geochemical and isotopic zoning patterns of plagioclase megacrysts in gabbroic dykes from the Gardar Province, South Greenland: implications for crystallisation processes in anorthositic magmas. Contrib. Mineral. Petrol. 144, 109–127.

Halama, R., Wenzel, T., Upton, B.G.J., Siebel, W., Markl, G., 2003. A geochemical and Sr–Nd–O isotopic study of the Proterozoic Eriksfjord Basalts, Gardar Province, South Greenland: reconstruction of an OIB-signature in crustally contaminated rift-related basalts. Min. Mag. 67, 831–854.

Halama, R., Vennemann, T., Siebel, W., Markl, G., in press. The Grønnedal-Ika carbonatite–syenite complex, South Greenland: an origin involving liquid immiscibility. J. Petrol.

Hawthorne, F.C., Ungaretti, L., Oberti, R., Bottazzi, P., 1993. Li: an important component in igneous alkali amphiboles. Am. Mineral. 78, 733–745.

Hawthorne, F.C., Ungaretti, L., Oberti, R., Cannillo, E., 1994. The mechanisms of [6]Li incorporation in amphiboles. Am. Mineral. 79, 443–451.

Irving, A.J., Frey, F.A., 1984. Trace element abundances in megacrysts and their host basalts: constraints on partition coefficients and megacryst genesis. Geochim. Cosmochim. Acta 48, 1201–1221.

Jeffries, T.E., Perkins, W.T., Pearce, N.J.G., 1995. Measurements of trace elements in basalts and their phenocrysts by laser probe microanalysis inductively coupled plasma mass spectrometry (LPMA-ICP-MS). Chem. Geol. 121, 131–144.

Jensen, B.B., 1973. Patterns of trace element partitioning. Geochim. Cosmochim. Acta 37, 2227–2242.

Jones, A.P., Peckett, A., 1980. Zirconium-bearing aegirines from Motzfeldt, South Greenland. Contrib. Mineral. Petrol. 75, 251–255.

Kalsbeek, F., Taylor, P.N., 1985. Isotopic and chemical variation in granites across a Proterozoic continental margin—the Ketilidian mobile belt of South Greenland. Earth Planet. Sci. Lett. 73, 65–80.

Klein, M., Stosch, H.-G., Seck, H.A., 1997. Partitioning of high field-strength and rare-earth elements between amphibole and quartz-dioritic to tonalitic melts: an experimental study. Chem. Geol. 138, 257–271.

Konnerup-Madsen, J., Rose-Hansen, J., 1984. Composition and significance of fluid inclusions in the Ilimaussaq peralkaline granite, South Greenland. Bull. Mineral. 107, 317–326.

Larsen, L.M., 1976. Clinopyroxenes and coexisting mafic minerals from the alkaline Ilimaussaq intrusion, South Greenland. J. Petrol. 17, 258–290.

Larsen, L.M., 1977. Aenigmatites from the Ilimaussaq intrusion, South Greenland: chemistry and petrological implications. Lithos 10, 257–270.

Larsen, L.M., 1979. Distribution of REE and other trace elements between phenocrysts and peralkaline undersaturated magmas, exemplified by rocks from the Gardar igneous province, South Greenland. Lithos 12, 303–315.

Larsen, L.M., 1981. Chemistry of feldspars in the Ilimaussaq augite syenite with additional data on some other minerals. Rapp.-Grønl. Geol. Unders. 103, 31–37.

Larsen, L.M., Sørensen, H., 1987. The Ilimaussaq intrusion—progressive crystallization and formation of layering in an agpaitic magma. In: Fitton, J.G., Upton, B.G.J. (Eds.), Alkaline Igneous Rocks, Spec. Publ.-Geol. Soc., vol. 30, pp. 473–488.

Larsen, L.M., Steenfelt, A., 1974. Alkali loss and retention in an iron-rich peralkaline phonolite dyke from the Gardar province, South Greenland. Lithos 7, 81–90.

Lemarchand, F., Villemant, B., Calas, G., 1987. Trace element distribution coefficients in alkaline series. Geochim. Cosmochim. Acta 51, 1071–1081.

Mahood, G., Hildreth, W., 1983. Large partition coefficients for trace elements in high-silica rhyolithes. Geochim. Cosmochim. Acta 47, 11–30.

Markl, G., Baumgartner, L., 2002. pH changes in peralkaline late-magmatic fluids. Contrib. Mineral. Petrol. 144, 31–346.

Markl, G., Marks, M., Wirth, R., 2001a. The influence of T, $aSiO_2$, f_{O2} on exsolution textures in Fe–Mg olivine: an example from augite syenite of the Ilimaussaq Intrusion, South Greenland. Am. Mineral. 86, 36–46.

Markl, G., Marks, M., Schwinn, G., Sommer, H., 2001b. Phase equilibrium constraints on intensive crystallization parameters of the Ilimaussaq complex, South Greenland. J. Petrol. 42, 2231–2258.

Marks, M., Markl, G., 2001. Fractionation and assimilation processes in the alkaline augite syenite unit of the Ilimaussaq intrusion, South Greenland, as deduced from phase equilibria. J. Petrol. 42, 1947–1969.

Marks, M., Markl, G., 2003. Ilimaussaq "en miniature": closed-system fractionation in an agpaitic dyke rock from the Gardar province, South Greenland. Min. Mag. 67, 893–919.

Marks, M., Vennemann, T.W., Siebel, W., Markl, G., 2003. Quantification of magmatic and hydrothermal processes in a peralkaline syenite–alkali granite complex based on textures, phase equilibria, and stable and radiogenic isotopes. J. Petrol. 44, 1247–1280.

Marks, M., Vennemann, T.W., Siebel, W., Markl, G., 2004. NCl^-, O^-, and H-isotopic evidence for complex, closed-system evolution of the peralkaline Ilímaussaq Intrusion, South Greenland. Geochim. Cosmochim. Acta 68, 3379–3395.

McDonough, W.F., Sun, S.S., 1995. The composition of the Earth. Chem. Geol. 120, 223–253.

Mitchell, R.H., 1990. A review of the compositional variation of amphiboles in alkaline plutonic complexes. Lithos 26, 135–156.

Nash, W.P., Crecraft, H.R., 1985. Partition coefficients for trace elements in silicic magmas. Geochim. Cosmochim. Acta 49, 2309–2322.

Nielsen, T.F.D., 1979. The occurrence and formation of Ti-aegirines in peralkaline syenites; an example from the Tertiary ultramafic alkaline Gardiner complex, East Greenland. Contrib. Mineral. Petrol. 69, 235–244.

Nimis, P., Vannucci, R., 1995. An ion microprobe study of clinopyroxenes in websteritic and megacrystic xenoliths from Hyblean Plateau (SE Sicily, Italy): constraints on HFSE/REE/Sr fractionation at mantle depth. Chem. Geol. 124, 185–197.

Njonfang, E., Nono, A., 2003. Clinopyroxene from some felsic alkaline rocks of the Cameroon Line, central Africa: petrological implications. Eur. J. Mineral. 15, 527–542.

Parsons, I., 1972. Petrology of the Puklen syenite–alkali granite complex, Nunarssuit, South Greenland. Medd. Grønl. 195 (73 pp.).

Pearce, N.J.G., Leng, M.J., Emeleus, C.H., Bedford, C.M., 1997a. The origins of carbonatites and related rocks from the Grønnedal-Ika nepheline syenite complex, South Greenland: C–O–Sr isotope evidence. Min. Mag. 61, 515–529.

Pearce, N.J.G., Perkins, W.T., Westgate, J.A., Gorton, M.P., Jackson, E.E., Neal, C.R., Chenery, S.P., 1997b. A compilation of new and published major and trace element data for NIST SRM 610 and NIST SRM 612 glass reference materials. Geostand. Newsl. 21, 115–144.

Piilonen, P.C., McDonald, A.M., Lalonde, A.E., 1998. The crystal chemistry of aegirine from Mont Saint-Hilaire, Quebec. Can. Mineral. 36, 779–791.

Poulsen, V., 1964. The sandstones of the Precambrian Eriksfjord Formation in South Greenland. Rapp.-Grønl. Geol. Unders. 2 (16 pp.).

Pulvertaft, T.C.R., 1961. The Puklen intrusion, Nunarssuit, SW Greenland. Medd. Grønl. 123, 35–49.

Ranløv, J., Dymek, R.F., 1991. Compositional zoning in hydrothermal aegirine from fenites in the Proterozoic Gardar Province, South Greenland. Eur. J. Mineral. 3, 837–853.

Rudnick, R., Fountain, D.M., 1995. Nature and composition of the Continental Crust: a lower crustal perspective. Rev. Geophys. 33, 267–309.

Schiano, P., Allegre, C.-J., Duprè, B., Lewin, E., Joron, J.-L., 1993. Variability of trace elements in basaltic suites. Earth Planet. Sci. Lett. 119, 37–51.

Semenov, E.I., Gerassimivsky, V.I., Maksimova, N.V., Andersen, S., Peteresen, O.V., 1965. Sørensenite, a new sodium–beryllium–tin–silicate from the Ilimaussaq intrusion, South Greenland. Bull.-Grønl. Geol. Unders. 61 (19 pp.).

Shannon, R.D., 1976. Revised effective ionic radii and systematic studies of interatomic distances in halides and chalcogenides. Acta Crystallogr., A 32, 751–767.

Shearer, C.K., Larsen, L.M., 1994. Sector-zoned aegirine from the Ilimaussaq alkaline intrusion, South Greenland: implications for trace-element behavior in pyroxene. Am. Mineral. 79, 340–352.

Thompson, G.M., Malpas, J., 2000. Mineral/melt partition coefficients of oceanic alkali basalts determined on natural samples using laser ablation-inductively coupled plasma-mass spectrometry (LAM-ICP-MS). Min. Mag. 64, 85–94.

Tiepolo, M., Vannucci, R., Oberti, R., Foley, S., Bottazzi, P., Zanetti, A., 2000a. Nb and Ta incorporation and fractionation in titanian pargasite and kaersurtite: crystal-chemical constraints and implications for natural systems. Earth Planet. Sci. Lett. 176, 185–201.

Tiepolo, M., Vannucci, R., Bottazzi, P., Oberti, R., Zanetti, A., 2000b. Partitioning of REE, Y, Th, U and Pb between pargasite, kaersutite and basanite to trachyte melts: implications for percolated and veined mantle. Geochem. Geophys. Geosyst. 1, 67–82.

Tiepolo, M., Tribuzio, R., Vannucci, R., 2002. The compositions of mantle-derived melts developed during the Alpine continental collision. Contrib. Mineral. Petrol. 144, 1–15.

Upton, B.G.J., Emeleus, C.H., 1987. Mid-Proterozoic alkaline magmatism in southern Greenland: the Gardar province. In: Fitton, J.G., Upton, B.G.J. (Eds.), Alkaline Igneous Rocks, Spec. Publ.-Geol. Soc. vol. 30. , pp. 449–471.

Upton, B.G.J., Emeleus, C.H., Heaman, L.M., Goodenough, K.M., Finch, A., 2003. Magmatism of the mid-Proterozoic Gardar Province, South Greenland: chronology, petrogenesis and geological setting. Lithos 68, 43–65.

Upton, B.G.J., Stephenson, D., Martin, A.R., 1985. The Tugtutùq older giant dyke complex: mineralogy and geochemistry of an alkali gabbro–augite–syenite–foyaite association in the Gardar Province of South Greenland. Min. Mag. 49, 624–642.

van Breemen, O., Aftalion, M., Allart, J.H., 1974. Isotopic and Geochronologic Studies on Granites from the Ketilidian Mobile Belt of South Greenland. Bull. Geol. Soc. Am. 85, 403–412.

Vannucci, R., Tribuzio, R., Piccardo, G.B., Ottolini, L., Bottazzi, P., 1991. SIMS analysis of REE in pyroxenes and amphiboles from the Proterozoic Ikasaulak intrusive complex (SE Greenland): implications for LREE enrichment processes during post-orogenic plutonism. Chem. Geol. 92, 115–133.

Villemant, B., Jaffrezic, H., Joron, J.-L., Treuil, M., 1981. Distribution coefficients of major and trace elements; fractional crystallization in the alkali basalt series of Chaine des Puys (Massif Central, France). Geochim. Cosmochim. Acta 45, 1997–2016.

Walter, A.V., Flicoteaux, R., Parron, C., Loubet, M., Nahon, D., 1995. Rare-earth elements and isotopes (Sr, Nd, O, C) in minerals from the Juquia carbonatite (Brazil); tracers of a multistage evolution. Chem. Geol. 120, 27–44.

White, J.C., 2003. Trace-element partitioning between alkali feldspar and peralkalic quartz trachyte to rhyolite magma: Part II. Empirical equations for calculating trace-element partition coefficients of large-ion lithophile, high field-strength, and rare-earth elements. Am. Mineral. 88, 330–337.

Witt-Eickschen, G., Harte, B., 1994. Distribution of trace elements between amphibole and clinopyroxene from mantle peridotites of the Eifel (western Germany): an ion-microprobe study. Chem. Geol. 117, 235–250.

Wood, B.J., Blundy, J.D., 1997. A predictive model for rare earth element partitioning between clinopyroxene and anhydrous silicate melt. Contrib. Mineral. Petrol. 129, 166–181.

Wood, B.J., Blundy, J.D., 2001. The effect of cation charge on crystal-melt partitioning of trace elements. Earth Planet. Sci. Lett. 188, 59–71.

Wood, B.J., Trigila, R., 2001. Experimental determination of aluminous clinopyroxene–melt partition coefficients for potassic liquids, with application to the evolution of the Roman province potassic magmas. Chem. Geol. 172, 213–223.

Wörner, G., Beusen, J.-M., Duchateau, N., Gijbels, R., Schmincke, H.-U., 1983. Trace element abundances and mineral/melt distribution coefficients in phonolites from the Laacher See Volcano (Germany). Contrib. Mineral. Petrol. 84, 152–173.